Published online 12 July 2022

Nucleic Acids Research, 2022, Vol. 50, No. 14 ***7991–8007***
https://doi.org/10.1093/nar/gkac581

In vitro reconstitution reveals a key role of human mitochondrial EXOG in RNA primer processing

Anna Karlowicz[1], Andrzej B. Dubiel[1], Jolanta Czerwinska[2,3], Adela Bledea[1], Piotr Purzycki[1], Marta Grzelewska[1], Ryan J. McAuley[4], Roman J. Szczesny[2], Gabriela Brzuska[5], Ewelina Krol[5], Bartosz Szczesny[4] and Michal R. Szymanski[1,*]

[1]Structural Biology Laboratory, Intercollegiate Faculty of Biotechnology of University of Gdansk and Medical University of Gdansk, University of Gdansk, ul. Abrahama 58, 80-307 Gdansk, Poland, [2]Institute of Biochemistry and Biophysics Polish Academy of Sciences, ul. Pawinskiego 5A, 02-106 Warsaw, Poland, [3]Faculty of Biology, Institute of Genetics and Biotechnology, University of Warsaw, Warsaw 02-106, Poland, [4]Department of Ophthalmology and Visual Sciences, The University of Texas Medical Branch, 301 University Boulevard, Galveston, TX 77555, USA and [5]Laboratory of Recombinant Vaccines, Intercollegiate Faculty of Biotechnology of University of Gdansk and Medical University of Gdansk, University of Gdansk, ul. Abrahama 58, 80-307 Gdansk, Poland

Received November 19, 2021; Revised June 01, 2022; Editorial Decision June 13, 2022; Accepted June 24, 2022

ABSTRACT

The removal of RNA primers is essential for mitochondrial DNA (mtDNA) replication. Several nucleases have been implicated in RNA primer removal in human mitochondria, however, no conclusive mechanism has been elucidated. Here, we reconstituted minimal *in vitro* system capable of processing RNA primers into ligatable DNA ends. We show that human 5′-3′ exonuclease, EXOG, plays a fundamental role in removal of the RNA primer. EXOG cleaves short and long RNA-containing flaps but also in cooperation with RNase H1, processes non-flap RNA-containing intermediates. Our data indicate that the enzymatic activity of both enzymes is necessary to process non-flap RNA-containing intermediates and that regardless of the pathway, EXOG-mediated RNA cleavage is necessary prior to ligation by DNA Ligase III. We also show that upregulation of EXOG levels in mitochondria increases ligation efficiency of RNA-containing substrates and discover physical interactions, both *in vitro* and *in cellulo,* between RNase H1 and EXOG, Pol γA, Pol γB and Lig III but not FEN1, which we demonstrate to be absent from mitochondria of human lung epithelial cells. Together, using human mtDNA replication enzymes, we reconstitute for the first time RNA primer removal reaction and propose a novel model for RNA primer processing in human mitochondria.

INTRODUCTION

Since the discovery that the instability of mitochondrial genome causes a wide variety of detrimental human disorders (1), the mechanisms of mitochondrial DNA (mtDNA) replication and repair have been studied extensively. Mitochondrial disorders originate from either mtDNA mutations or defective nuclear genes coding for proteins that function in mitochondria (2), including nuclear-encoded components involved in the metabolism of mtDNA. Mammalian mtDNA is a small (16.6 kb), circular, double-stranded DNA molecule encoding 13 proteins that constitute a minority amongst the tens of the oxidative phosphorylation (OXPHOS) subunits encoded by nuclear genes. Still, mtDNA expression is essential for the respiratory chain (3), therefore, proper function of mitochondria requires effective maintenance of mtDNA, i.e. DNA replication and DNA damage repair (4).

DNA polymerase Pol γ is exclusive to mitochondria (5) and functions in both mtDNA replication and repair (5,6). Human Pol γ is a holoenzyme consisting of a catalytic subunit Pol γA and a dimeric accessory subunit Pol γB. Enzymatic activities of Pol γA include polymerization for DNA synthesis, 3′–5′ exonuclease for proofreading and 5′-dRP lyase for DNA repair (6–8). Pol γ can form short 5′-flaps due to its intrinsic ability to displace downstream DNA or RNA encountered during mtDNA synthesis (9,10). Even though Pol γ displays limited strand displacement activity *in vitro*, inactivation of its exonuclease activity leads to excessive formation of unligatable 5′-flaps (9,11,12). Over 300 pathogenic mutations in the genes coding for both Pol γA and γB subunits were identified, including mutations that alter the exonuclease activity of human Pol γ (2,12).

*To whom correspondence should be addressed. Tel: +48 58 523 63 66; Fax: +48 58 523 64 27; Email: michal.szymanski@ug.edu.pl

There are three models of mtDNA replication that are currently proposed (for recent reviews, refer to (13,14)). The original model of mtDNA replication emerged in early 1970s. It assumed a strand-displacement mechanism deduced from electron microscopy analyses of replicative intermediates of mammalian mtDNA (15–17). The model proposes that the leading strand synthesis starts at the origin of replication on the heavy strand (known as O_H). When the replication fork reaches approximately two-thirds of the length of mtDNA genome, the second origin of replication on the light strand (known as O_L) is exposed allowing the other strand synthesis in the opposite direction. Termination of mtDNA replication requires the removal of the RNA primers present at the 5′-ends of the nascent strands (18). Pol γ-driven RNA primer displacement, flap formation and its eventual removal at the origins of DNA replication are critical steps preceding nicks ligation to complete DNA synthesis (19,20).

Several nucleases have been proposed to be involved in mitochondrial RNA primer removal. RNase H1 was indicated to be essential in this process (21). However, it was shown to be insufficient as it leaves behind a few (1–3 nt) ribonucleotides at the RNA–DNA junction (22,23). Therefore, it was proposed that a secondary nuclease is required to complete primer removal and allow for ligation to terminate mtDNA replication. FEN1, a well-known flap nuclease involved in Okazaki fragments maturation in the nucleus (24–28) was proposed to be involved in mitochondrial primer removal. However, the role of FEN1 in mitochondria is controversial (29,30), therefore, it was concluded that a FEN1-like enzyme remained unidentified (23). Dna2, a flap nuclease/helicase (24–28) fails to generate ligatable substrate for Lig III (23). A mitochondrial flap nuclease MGME1 is unable to cleave RNA (10,31). Therefore, the identity of nuclease that removes the remining RNA during replication of mtDNA is currently unknown.

Human nuclease EXOG (EXOG) is an evolutionarily conserved 5′-3′ exonuclease exclusively localized in mitochondria (32). Both *in vivo* and *in vitro* studies indicated critical role of EXOG in mtDNA integrity and mitochondrial function. EXOG depletion induces persistent single stranded DNA breaks (SSBs) in the mtDNA, enhances ROS levels, causes mitochondrial dysfunction and cell death in HeLa and MCF7 cell lines (33), while ectopic expression of EXOG improves the cellular resistance to oxidative challenge (34). Recently, a protective role of EXOG in mtDNA stability and mitochondrial functional maintenance was confirmed in rotenone treated neuronal PC12 cells (35). Structural and biochemical analysis of EXOG revealed a distinct mechanism for substrate recognition and a specific exonuclease activity that allows processing of the 5′-end of DNA downstream of the damage, providing an optimal substrate for efficient DNA base-excision repair (BER) (36). Additionally, it was shown that, besides DNA lesions processing, EXOG cleaves ssDNA, ssRNA and RNA in an RNA/DNA hybrid duplex (37), suggesting its putative role in a non-flap primer removal in mitochondria.

In this study, we investigated the involvement of EXOG in the process of RNA primer removal. We show that in a flap–dependent pathway, EXOG cleaves both short and long RNA-containing flaps, deleterious strand displacement intermediates generated by Pol γ that could otherwise compromise the mtDNA integrity. We discover physical interaction between EXOG and RNase H1, both *in vitro* and *in cellulo*, and demonstrate that coordinated action of these two nucleases is critical in a flap-independent pathway to process non-flap RNA structures resistant to RNase H1 cleavage. We show that upregulation of EXOG in mitochondrial extracts enhances ligation efficiency of nonligatable DNA/RNA intermediates. Additionally, we detect both *in vitro* and *in cellulo* interactions between RNase H1 and Pol γ as well as Lig III but not FEN1. Importantly, we show that regardless of the pathway, nucleolytic activity of EXOG generates RNA-free intermediate products that are successfully ligated by Lig III thus allowing us, for the first time, to reconstitute RNA primer removal reaction *in vitro* exclusively with human mtDNA replication components. Collectively, our results indicate that EXOG is essential for complete RNA primer removal *in vitro*, therefore, we propose that EXOG could play a role during replication of the mtDNA.

MATERIALS AND METHODS

Protein purification

hEXOG-ΔN58 and hEXOG-ΔN58/H140G are recombinant proteins lacking mitochondrial localization sequence (MLS) and were purified as previously described (36) with the following modifications: the IPTG-induced culture was grown for 4 h at 37°C; the enzyme was stored in buffer containing 20 mM HEPES pH 8.0, 300 mM KCl, 1 mM TCEP and 50% (v/v) glycerol. The concentration was determined spectrophotometrically using extinction coefficient $\varepsilon_{280(\text{dimer})} = 77\ 030\ \text{M}^{-1}\ \text{cm}^{-1}$. Analytical size exclusion chromatography (Superdex 200 Increase 10/300 GL column, GE Healthcare) was performed as a quality control step to compare oligomeric state of EXOG variants.

The pET-11a-based construct coding for non-tagged mature human mtSSB (amino acids 18–148) (Epoch) was transformed into *Escherichia coli* BL21 Rosetta (DE3) (Novagen). Overnight culture was diluted into fresh LB media supplemented with ampicillin (100 μg/ml) and chloramphenicol (30 μg/ml) and grown at 37°C to an OD_{600} of 0.8. hmtSSB overproduction was induced with IPTG (final concentration of 1 mM) and further grown for 3 h at 30°C. Cell lysis was performed by sonication in buffer containing 40 mM Tris–HCl pH 7.5, 8% (w/v) sucrose, 200 mM NaCl, 2 mM EDTA and 2% (w/v) sodium cholate. The lysate was centrifuged at 75 000 × g for 30 min at 4°C and the collected supernatant was loaded onto the Blue Sepharose 6 Fast Flow resin (GE Healthcare) equilibrated with 35 mM Tris–HCl pH 7.5, 200 mM NaCl, 2 mM EDTA and 10% (v/v) glycerol buffer. The flow-through fractions containing hmtSSB were pooled and the ammonium sulfate precipitation was performed as previously described (38). The final precipitate was suspended and dialysed against SQ buffer (50 mM CAPS pH 9.7, 200 mM NaCl, 2 mM EDTA, 2 mM BME, 10% (v/v) glycerol). Further, protein was loaded onto the Q Sepharose Fast Flow resin (GE Healthcare) equilibrated with the SQ buffer. The flow-through fractions con-

taining hmtSSB were pooled and dialysed against the SQ buffer but with 50 mM NaCl. The same Q resin equilibrated with the 50 mM NaCl SQ buffer was loaded with hmtSSB, washed with the same buffer and the protein was eluted with a linear gradient of NaCl (0.05–0.5 M). The hmtSSB-containing elution fractions were pooled, dialysed against 20 mM HEPES pH 8.0, 140 mM KCl, 1 mM TCEP and 5% (v/v) glycerol buffer and loaded onto a Hi-Load 16/600 Superdex 200 gel filtration column (GE Healthcare). The peak fractions were pooled and the concentration was determined spectrophotometrically using extinction coefficient $\varepsilon_{280(\text{tetramer})} = 79\ 760\ \text{M}^{-1}\ \text{cm}^{-1}$.

Human RNase H1 (amino acids 27–286) with an N-terminal thrombin-cleavable His_6 tag was overproduced from pET15b construct (a gift from Dr Marcin Nowotny from International Institute of Molecular and Cell Biology, Poland) in *Escherichia coli* BL21 (DE3) pLysS (Novagen). The pET15b-encoded variant protein RNase H1-D210N with an N-terminal thrombin-cleavable His_6 tag (Epoch) was overproduced in *E. coli* BL21 (DE3) (Novagen). Both proteins were purified as previously described (39) with modifications. The buffers contained 20 mM HEPES pH 7.0 instead of 40 mM NaH_2PO_4. The stepwise elution from Ni-NTA resin (Macherey-Nagel) was performed with 300 mM imidazole instead of a linear gradient. After His_6 tag cleavage, wild-type RNase H1 was loaded onto Ni-NTA resin. The unbound, tag-free protein was collected and loaded onto a Hi-Load 16/600 Superdex 200 gel filtration column (GE Healthcare) equilibrated with 20 mM HEPES pH 7.0, 100 mM NaCl, 0.5 mM EDTA and 5% (v/v) glycerol buffer. For the mutant protein, the His_6 tag cleavage was followed by a Mono S 5/50 GL column (GE Healthcare) chromatography. The stepwise elution was performed with 1 M NaCl instead of a linear gradient. The mutant protein-containing fractions were collected and loaded onto a HiPrep 16/60 Sephacryl S-300 HR gel filtration column (GE Healthcare). The concentration was determined spectrophotometrically using extinction coefficient $\varepsilon_{280} = 47\ 565\ \text{M}^{-1}\ \text{cm}^{-1}$. Analytical size exclusion chromatography (Superdex 200 Increase 10/300 GL column) was performed as a quality control step to assess the oligomeric state of RNase H1 variants.

The full-length human Lig IIIα protein (lacking MLS) was overproduced from a modified pET28 plasmid containing an N-terminal His_6-SUMO tag (a gift from Dr P.J. O'Brien from University of Michigan) in *E. coli* BL21 Rosetta (DE3) cells as previously described (40). The concentration was determined spectrophotometrically using extinction coefficient $\varepsilon_{280} = 79\ 988\ \text{M}^{-1}\ \text{cm}^{-1}$.

The Pol γA-coding gene (encoded protein lacks MLS and 10 of the 13 sequential glutamine residues 43–52) was transferred into the baculovirus genome using the shuttle vector pBacPak9 (Clontech). The C-terminal His-tagged protein was synthesized in Sf9 insect cells (Invitrogen), infected at a density of 1–2 × 10^6 cells/ml and grown at 27°C in SF900-II SFM growth medium (Gibco). After 72 h cells were harvested by centrifugation at 500 × g, washed in growth medium and frozen in liquid nitrogen. Cells were gently resuspended in the lysis buffer (15 mM HEPES pH 7.6, 250 mM sucrose, 75 mM KCl, 2.25 mM $CaCl_2$, 1.5 mM magnesium acetate, 1.25% (v/v) glycerol, 0.375% (v/v) NP-40, 0.025% (v/v) Triton X-100). The lysate was centrifuged at 1500 × g for 10 min. The collected supernatant was mixed gradually with KCl buffer (2 M KCl, 20 mM HEPES pH 8.0, 5% (v/v) glycerol) to the final KCl concentration of 0.5 M. After 30 min of mixing, the lysate was centrifuged at 31 000 × g for 30 min. Pol γA was purified by sequential application of Talon Superflow resin (GE Healthcare) (elution with 200 mM imidazole) and a Hi-Load 16/600 Superdex 200 gel filtration column as previously described (41). The concentration was determined spectrophotometrically using extinction coefficient $\varepsilon_{280} = 242\ 295\ \text{M}^{-1}\ \text{cm}^{-1}$.

The His-tagged recombinant Pol γB protein was overproduced from pET22b + vector (Epoch, based on 6) in *E. coli* BL21 Rosetta II (DE3) pLysS cells (Novagen) as previously described (42) with the following modifications: pellet from 1 liter of bacterial culture was used and cells were lysed by sonication; the lysate was adjusted to contain 10 mM imidazole and no $MgCl_2$ before Ni-NTA resin binding; gel filtration chromatography was performed with a Superdex 200 Increase 10/300 GL column equilibrated with 20 mM HEPES pH 7.5, 140 mM KCl, 5 mM BME and 5% (v/v) glycerol buffer. The concentration was determined spectrophotometrically using extinction coefficient $\varepsilon_{280(\text{dimer})} = 143\ 280\ \text{M}^{-1}\ \text{cm}^{-1}$.

The full-length human FEN1 (amino acids 2−380) with an N-terminal His_6-SUMO tag was overproduced from the pE-SUMO vector (a gift from Prof. Jane A. Grasby from University of Sheffield, UK) in *E. coli* BL21 Rosetta II (DE3) pLysS cells (Novagen). Overnight culture was diluted into fresh 2xYT media containing 34 μg/mL chloramphenicol and 25 μg/ml kanamycin and grown at 30°C to an OD_{600} of 0.5. FEN1 overproduction was induced with IPTG (final concentration of 0.4 mM) and further grown for 16 h at 16°C. Cells were lysed by sonication in buffer containing 20 mM Tris–HCl pH 7.0, 1 M NaCl, 5 mM imidazole and 0.1% (w/v) lysozyme. The lysate was centrifuged at 12 000 × g for 30 min at 4°C and the collected supernatant was loaded onto the Talon Superflow resin equilibrated with 20 mM Tris–HCl pH 7.0, 1 M NaCl and 5 mM imidazole buffer. The resin was washed with 20 mM Tris–HCl pH 7.0, 500 mM NaCl, 40 mM imidazole and 0.1% (v/v) Tween 20 buffer and the protein was one-step eluted with 20 mM Tris–HCl pH 7.0, 1 M NaCl and 250 mM imidazole buffer. Fractions containing FEN1 were pooled and the His_6-SUMO tag was digested using SUMO protease (Ulp1) prior to loading onto the Talon Superflow resin. A flow-through fraction with cleaved FEN1 protein was collected and diluted to a final NaCl concentration of 250 mM with 20 mM Tris–HCl pH 8.0 and 1 mM EDTA buffer and $CaCl_2$ was added to the final concentration of 2 mM. FEN1 was loaded onto a HiTrap Heparin HP column (GE Healthcare) equilibrated and washed with 25 mM Tris–HCl pH 7.5 and 1 mM $CaCl_2$ buffer and the protein was eluted with a linear gradient of NaCl (0–1 M). The FEN1-containing elution fractions were pooled and loaded onto the HiPrep 16/60 Sephacryl S-300 HR column equilibrated with 50 mM HEPES pH 7.5, 1 mM $CaCl_2$, 100 mM KCl, 5 mM DTT and 10% (v/v) glycerol buffer. The peak fractions were pooled and dialyzed against 50 mM HEPES pH 7.5, 1 mM $CaCl_2$, 100 mM KCl, 5 mM DTT and 40% (v/v) glycerol buffer. The concentration was deter-

mined spectrophotometrically using extinction coefficient $\varepsilon_{280} = 23{,}107\ M^{-1}\ cm^{-1}$.

Labeling of EXOG and RNase H1 with fluorescent dye

Purified His-tagged hEXOG-ΔN58 and hEXOG-ΔN58/H140G were labeled using Alexa Fluor 647 Maleimide (Invitrogen). Protein was bound to Ni-NTA resin and washed with buffer EL (20 mM HEPES pH 7.5, 300 mM NaCl, 10% (v/v) glycerol) to remove reducing agent. Ni-NTA-bound protein was incubated with Alexa Fluor 647 maleimide at the molar ratio of EXOG:Alexa = 1:8 at 4°C overnight. The reaction was stopped, and the excess dye was washed away with buffer EL supplemented with 5 mM BME. The stepwise elution from Ni-NTA resin was performed with 200 mM imidazole in buffer EL + BME. The labeled protein was further loaded onto a Superdex 200 Increase 10/300 GL column equilibrated with buffer EL + BME. The concentration of the protein was determined spectrophotometrically using extinction coefficient $\varepsilon_{280(dimer)} = 77\ 030\ M^{-1}\ cm^{-1}$ after correction for the dye contribution at 280 nm. The degree of labeling (1 dye molecule per EXOG dimer) was determined comparing with the concentration of the dye calculated using $\varepsilon_{652} = 265\ 000\ M^{-1}\ cm^{-1}$. Purified RNase H1 ($His_6$ tag-cleaved) was labeled with Alexa Fluor 647 NHS Ester (Invitrogen). Protein was incubated with the dye at the molar ratio of RNase H1:Alexa = 1:3 at 4°C for 1 h. The excess dye was washed away by dialysis with buffer RL (20 mM HEPES pH 7.0, 100 mM NaCl, 5% (v/v) glycerol, 2 mM DTT, 0.5 mM EDTA) at 4°C overnight. The labeled protein was further loaded onto a Superdex 200 Increase 10/300 GL column equilibrated with buffer RL (200 mM NaCl). The concentration of the protein was determined spectrophotometrically using extinction coefficient $\varepsilon_{280} = 47\ 565\ M^{-1}{\cdot}cm^{-1}$ after correction for the dye contribution at 280 nm. The degree of labeling (1 dye molecule per RNase H1 monomer) was determined comparing with the concentration of the dye calculated using $\varepsilon_{650} = 239\ 000\ M^{-1}\ cm^{-1}$.

Preparation of RNA and DNA substrates

All the oligonucleotides used in this study were purchased from Metabion International AG and are listed in Supplementary Table S1. The annealing of substrates (listed in Supplementary Table S2) was performed at 95°C for 5 min in TE buffer (20 mM Tris–HCl pH 8.1, 0.1 mM EDTA) and slowly cooled to room temperature. The downstream oligonucleotide of each linear substrate was 3′-end labeled with fluorescein. A circular template was obtained by the circularization of a 110-nt oligonucleotide (B5, Supplementary Table S1) with ssDNA Ligase (CircLigase II, Epicentre).

Exonuclease activity assay

Details on each reaction conditions are given in the figure legends. Reactions were initiated by the addition of an equal volume of fluorescein-labeled substrates (listed in Supplementary Tables S1 and S2). All experiments were performed at room temperature in Buffer HK140 (20 mM HEPES pH 7.5, 140 mM KCl, 1 mM TCEP, 0.1 mg/ml BSA). Reactions were stopped by the addition of BF Stop (78% (v/v) formamide, 50 mM EDTA, 0.1% (w/v) SDS), followed by incubation at 95°C for 4 min. Cleavage products were resolved by denaturing polyacrylamide gel electrophoresis and visualized using Typhoon fluorescence imager. When indicated, substrate bands were quantified using ImageJ (http://rsb.info.nih.gov/ij/).

Ligation assay

Reaction mixtures contained 200 nM fluorescein-labeled nicked substrate (substrates depicted in the figures), 200 nM Lig IIIα, 5 nM EXOG and/or RNase H1, 150 nM Pol γA, 600 nM Pol γB in Buffer HK140 supplemented with 10 mM $MgCl_2$, 1 mM ATP, 1 mM dNTPs and 1.89 μM Streptavidin (New England BioLabs). After 10 min incubation at 37°C, unlabeled competitor DNA oligonucleotide C1 (Supplementary Table S1) was added to the final concentration of 10 μM, followed by further incubation at 37°C for 1 h. Reactions were stopped by the addition of 2× BF Stop, incubated at 95°C for 4 min, cooled down on ice, resolved by 23%/7 M UREA/0.5× TBE denaturing polyacrylamide gel electrophoresis and imaged with Typhoon fluorescence imager. When indicated, product bands were quantified using ImageJ.

Primer extension-ligation assay

Reaction mixtures containing 2.5 nM substrate (primed substrates depicted in the figures), 12.5 nM Pol γA, 25 nM Pol γB and 2.5 nM hmtSSB in Buffer HK140 supplemented with 10 mM $MgCl_2$, 1 mM ATP, 0.5 μM unlabeled dNTPs and 2.5 nM [α-^{32}P] dCTP (800 Ci/mmol, 10 mCi/ml; Hartmann Analytic) were preincubated for 20 min at 37°C, followed by the addition of 25 nM Lig IIIα, 750 pM EXOG and/or 750 pM RNase H1 and further incubation at 37°C for 1 h. The reactions were stopped by the addition of Proteinase K (A&A Biotechnology) to the final concentration of 200 μg/ml and incubated at 48°C for 1 h. Where indicated, reactions were further treated with 300 mM KOH for 2 h at 55°C. Finally, all reactions were stopped by the addition of 2x BF Stop, incubated at 65°C for 2 min, cooled down on ice and resolved by 12%/7 M UREA/1× TBE denaturing polyacrylamide gel electrophoresis. Gels were dried and visualized using Typhoon phosphorimager. When indicated, product bands were quantified using ImageJ.

Microscale thermophoresis (MST)

The binding affinity of RNase H1 and EXOG with their potential partners was measured at 25°C using Microscale thermophoresis (MST) with Monolith NT.115 (NanoTemper): Excitation Nano-RED, 70–100% Excitation Power and Medium MST-Power. Depending on the target, MST-on (hot region) or MST-off (Initial Fluorescence-IF) was applied (for details on a technique, refer to (43)). Alexa 647-labeled RNase H1 and EXOG at a final concentration of 10 and 2 nM, respectively, were used as targets. The increasing concentration (10 pM–5.1 μM) of purified proteins

were used as ligands (EXOG, RNase H1, Pol γA, Pol γB, Lig III or FEN1). Measurements were carried out in PBS pH 7.6 buffer with 0.05% (v/v) NP-40 for RNase H1 target or 0.05% (v/v) Tween 20 for EXOG target. To prevent adsorption of the samples, premium coated capillaries were used (NanoTemperTechnologies). In MST analysis of EXOG target, a ligand-dependent change in the initial fluorescence was observed. To confirm that the change in the initial fluorescence was due to the interaction between the target and the ligand (not because of non-specific binding effects), the SD-Test (denaturation test) was performed (according to the manufacturer's instructions). Upon the disruption of the target-ligand interaction (via denaturation) no changes in the fluorescence intensities between the target and complex samples were observed (Supplementary Figure S15). The dissociation constant was determined using a single-site model with MO Affinity Analysis software version 2.3. All the results of the MST analysis, MST-on (Fnorm [‰]) and MST-off (Fluorescence [counts]), are presented as a Fraction Bound [-] (43,44).

Cell culture and stable cell lines generation

Human non-tumorigenic bronchial lung epithelial cells (BEAS 2B; ATCC CRL-9609) were maintained in RPMI 1640 medium supplemented with 10% FBS at 37°C in 5% CO_2. Mitochondria for mitoplasts preparation were isolated from the 293 Flp-In T-REx cells (Thermo Fisher Scientific, # R78007) or their stably transfected derivatives established in this study. Cells were cultured in Dulbecco's-modified Eagle's medium (DMEM, HyClone) supplemented with 10% FBS at 37°C in 5% CO_2. Stable cell lines were developed based on the protocols described previously (45). DNA constructs for stable cell lines generation were prepared using SLIC (sequence and ligation independent cloning) method similarly as described previously (45). Applied DNA constructs are listed in Supplementary Table S3. Expression of the transgenes was induced with tetracycline (7.5 ng/ml).

Mitochondria isolation and mitoplasts preparation

Mitochondria isolation followed by mitoplasts preparation was performed as described previously (46). Briefly, cells were harvested by centrifugation at 400 × g for 4 min at 4°C in NKM buffer (1 mM Tris–HCl, pH 7.4, 0.13 M NaCl, 5 mM KCl, 7.5 mM $MgCl_2$). The cell pellet was suspended in ice-cold 0.1× HomB buffer (4 mM Tris–HCl, pH 7.6, 2.5 mM NaCl, 0.5 mM $MgCl_2$) and cells were homogenized in a Dounce homogenizer. The cell homogenate was supplemented with 10x HomB buffer to obtain 1× HomB (40 mM Tris–HCl pH 7.6, 25 mM NaCl, 5 mM $MgCl_2$). The homogenate was centrifuged three times at 900 × g for 4 min at 4°C to remove nuclei and cell debris. Mitochondria were pelleted by centrifugation at 8000 × g for 5 min at 4°C. To prepare mitoplasts, isolated mitochondria were resuspended in 1× HomB buffer, incubated with 0.1% (w/v) digitonin (Sigma-Aldrich, # D5628) for 10 min on ice and centrifuged at 7000 × g for 2.5 min at 4°C. The resultant pellets were resuspended in 1× HomB buffer with 0.1 mg/ml Proteinase K (Thermo Fisher Scientific, # EO0491), incubated on ice for 20 min and centrifuged at 7000 × g for 2.5 min at 4°C. Pellets were resuspended in 1× HomB buffer supplemented with 2 mM PMSF and protease inhibitor cocktail to inhibit Proteinase K. After pelleting, resuspending in 1x HomB buffer and re-pelleting, intact mitoplasts were lysed in lysis buffer (20 mM HEPES–NaOH, pH 7.4, 1 mM EDTA, 1 mM DTT, 300 mM KCl, 5% (v/v) glycerol and 0.2% (v/v) NP-40) supplemented with 0.25 mM PMSF and protease inhibitor cocktail. Protein concentration was measured using the Bradford method. The mitoplast extracts were aliquoted, snap-frozen in liquid nitrogen, and stored at −80°C until used for ligation assay.

Ligation assay with mitoplast extracts

Reaction mixture contained 40 mM HEPES pH 7.8, 0.1 mM EDTA, 10 mM $MgCl_2$, 0.2 mg/ml BSA, 50 mM KCl, 3% (v/v) glycerol, 1 mM DTT, 2 mM ATP, 200 μM dNTPs, 15–20 μg of mitoplast extract and 100 nM fluorescein-labeled substrate (depicted in the figure). Due to undetectable efficiency of parental extracts in ligation reaction with non-flap substrate containing 2RNA-18DNA chimeric strand, after 2 h incubation at 37°C, Lig III was added to the final concentration of 400 nM followed by further incubation at 37°C for 20 min. Reactions were stopped by the addition of Proteinase K and SDS to the final concentration of 0.6 mg/mL and 0.5% (w/v), respectively, and incubated at 55°C for 30 min. Finally, all reactions were stopped by adding 2× Loading Stop BF (90% (v/v) formamide, 20 mM EDTA), incubated at 85°C for 5 min, cooled down on ice and resolved by 20%/7 M UREA/1× TBE denaturing polyacrylamide gel electrophoresis. Gels were visualized using Typhoon fluorescence imager and product bands were quantified using MultiGauge software.

Cellular EXOG level analysis

Whole cell extracts were prepared in RIPA lysis buffer (10 mM Tris–HCl pH 7.4, 140 mM NaCl, 5 mM EDTA, 1% (v/v) Triton X-100, 1% (w/v) sodium deoxycholate and 0.1% (w/v) SDS) supplemented with 0.25 mM PMSF and protease inhibitor cocktail. Protein concentration was measured by the Bradford method using the protein assay dye reagent (Bio-Rad, #5000006). Equal amounts of extracts (30 μg) were separated by SDS-PAGE and subsequently probed with primary antibodies to detect EXOG (Supplementary Table S4).

Proximity ligation assay (PLA)

PLA was performed using a pair of primary antibodies raised in two different species according to manufacturer's instruction of the Duolink In Situ Kit (Sigma-Aldrich, #DUO92002). Briefly, BEAS 2B cells were seeded at a density of 20 000 cells/well in Lab-Tek Chamber Slides w/Cover (Thermo Scientific, #178599) and incubated at 37°C in 5% CO_2 for 24 h. Cells were fixed and permeabilized with 4% paraformaldehyde, 0.2% Tween-20 in PBS for 20 min. After three washes with PBS, primary antibodies (details in Supplementary Table S4) recognizing the following targets were used: RNase H1, EXOG, FEN1, Lig III,

Pol γA, Pol γB, COX IV (source in Supplementary Table S4) and dsDNA (source in Supplementary Table S4). The binary interaction (close proximity) between proteins was visualized using a red fluorescent signal. Images were captured using a Nikon Eclipse 80i inverted fluorescent microscope with Photometric CoolSNAP HQ2 camera and NIS-Elements BR 3.10 software.

Mitochondrial fractionation

The 1×10^7 of BEAS 2B cells were used for mitochondrial fractionation to obtain two fractions containing the mitochondrial outer membrane + intermembrane space (OM + IMS) and mitochondrial inner membrane (IM) + matrix as described in (47). 20 μg of each fraction, whole cell extract (WCE), cytoplasm, and two mitochondrial subfractions were separated by SDS-PAGE and subsequently probed with primary antibodies (details in Supplementary Table S4) recognizing the following targets: RNase H1, EXOG, Pol γA, Pol γB, Lig III, FEN1, α subunit of ATP synthase, TIM22, TOM22, β-actin and cytochrome *c*.

RESULTS

EXOG cleaves ssRNA of various lengths

Human EXOG was previously shown to cleave single-stranded DNA and RNA substrates with higher efficiency as compared to duplex structures (32,36,37). To address functional implications of this broad spectrum of activities we purified the hEXOG-Δ58 truncation mutant (previously described by us in (36)) lacking 58 amino acids at the N-terminus which constitute mitochondrial localization sequence (MLS), trans-membrane domain and a predicted unstructured region (Supplementary Figure S1). Since EXOG is a 5′-3′ exonuclease, we used DNA and RNA substrates labeled at 3′-end with fluorescein and confirmed that under identical experimental conditions the hEXOG-Δ58 variant (further referred to as EXOG) cleaves single-stranded substrates (both ssDNA and ssRNA) with significantly higher efficiency than gapped DNA:DNA and RNA:DNA duplexes (Supplementary Figure S2).

Very efficient ssRNA cleavage by EXOG and the ability of Pol γ to displace several nucleotides of the downstream RNA (10) led us to investigate whether the length of ssRNA affects the cleavage efficiency by EXOG. To avoid potential sequence-dependent cleavage site preferences of EXOG, we examined nucleolytic activity of EXOG using homooligonucleotides of different length: U_5, U_{10}, U_{20} and U_{30} in the time-course experiment. We found that 10-mer and longer ssRNA oligonucleotides were cleaved with similar efficiency as 50% of the initial amount of substrate was cut after 5 min of the reaction time (Figure 1A and B). Interestingly, the cleavage was very rapid even though the reactions were performed at large excess of substrates over enzyme (400 nM of the substrate and 0.1 nM of EXOG). This could be explained by the fact that polyU, unlike heterooligomeric RNA or any ssDNA molecules, does not form secondary structures at physiological conditions (48), therefore, is likely to be readily targeted to the active site of EXOG. The shortest ssRNA oligomer tested (5-nt long) was more resistant to EXOG degradation as 50% of the substrate was cleaved in >30 min (Figure 1B). Based on the recent crystal structure of the EXOG-dsRNA/DNA complex (PDB: 5ZKJ) (37) we modelled EXOG-ssRNA interactions and show that EXOG interacts with 5 nt of RNA from the 5′-end (Figure 1C). Presumably, with each consecutive cut, interactions between EXOG and progressively shorter ssRNA are lost, thus explaining lower cleavage efficiency of 5-nt RNA substrate as compared to longer ssRNA oligomers.

EXOG efficiently removes RNA flaps

It has been shown that Pol γ forms short 5′-flaps due to its limited intrinsic ability to displace downstream DNA or RNA encountered during mtDNA synthesis (9,10). Since our results showed that EXOG efficiently cleaves ssRNA of various lengths, next we tested its ability to process substrates that mimic the flap-dependent pathway of RNA primer removal and analyzed various nicked substrates containing downstream 5′ RNA flaps with fluorescently labeled 3′ end (Figure 2A and B). All the unlabeled blunt ends in linear substrates used in this study are blocked with biotin. First, we tested the cleavage activity of EXOG on a short 2-nt long RNA (2RNA) flap and compared its processing to a non-flap, nicked substrate with downstream 2RNA-18DNA chimeric oligonucleotide. We found that EXOG cleaves 2RNA flap very efficiently (Figure 2A, lanes 2–6), pausing at the bottom of the flap (as a 20-nt band is a dominant product, lanes 4 and 5) thus generating the optimal substrate for ligation. A limited activity of EXOG was displayed on the non-flap, nicked substrate (Figure 2A, lanes 24–28), which is in line with recently published data (37). To compare the activity of RNase H1 on the same substrate under the same experimental conditions, we purified RNase H1 (Supplementary Figure S3) and show that it cleaves neither 2RNA flap (Figure 2A, lanes 7–11) nor non-flap 2RNA-18DNA chimera (Figure 2A, lanes 29–33). We then analyzed if longer RNA-containing flaps are also susceptible to the EXOG-mediated cleavage. Flaps consisting solely of RNA (15U and heterogeneous 15RNA flaps) were cleaved very efficiently (Figure 2B, lanes 2–6 and 14–18, respectively). At 100 nM concentration of EXOG both RNA flaps were removed completely generating a nicked product optimal for ligation (Figure 2B, lanes 5 and 17), similarly to the short 2RNA flap cleavage (Figure 2A, lane 5). In case of a chimeric 2RNA-13DNA flap we observed pausing at the RNA-DNA junction at the lowest concentration of EXOG (Figure 2A, lane 13) and further cleavage required higher enzyme concentration (Figure 2A, lanes 14–16). In contrast to RNA flaps, the chimeric flap removal did not generate the optimal substrate for ligation. We observed accumulation of products shorter than 20 nt, which suggests that after flap removal EXOG cleaves out additional 1 or 2 nucleotides from the downstream DNA duplex (Figure 2A, lanes 14–16). In comparison, all long RNA-containing flaps were resistant to RNase H1 (Figure 2A, lanes 17–21; Figure 2B, lanes 7–11 and 19–23). Together, both short and long RNA flaps are efficiently removed by EXOG yet pausing of EXOG at the RNA-DNA junction in case of chimeric flaps contributes to reduced cleavage efficiency (Figure 2C).

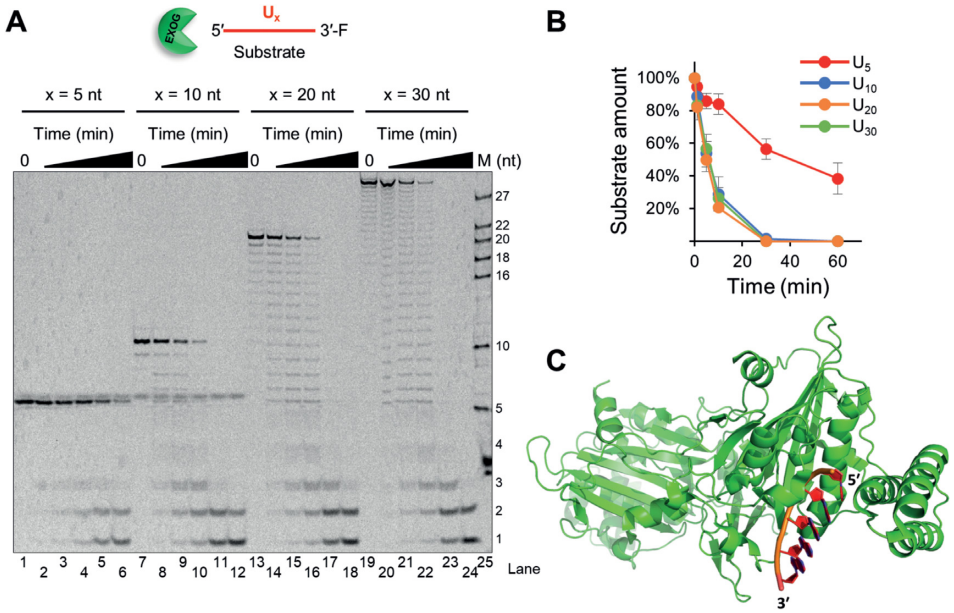

Figure 1. EXOG efficiently cleaves ssRNA of various lengths. (**A**) 400 nM of ssRNA (5-mer O3, 10-mer O4, 20-mer O5, 30-mer O6, Supplementary Table S1) was incubated with 0.1 nM EXOG. Reactions were stopped at indicated time points (0, 1, 5, 10, 30, 60 min) and analyzed on a 23% denaturing polyacrylamide gel. Corresponding molecular weight standards are marked with M. (**B**) Densitometric analysis of the decrease of tested substrates in (A). The graph presents the mean values with standard deviations (error bars) from two experiments. (**C**) Model of EXOG-ssRNA complex (based on crystal structure PDB: 5ZKJ) shows that EXOG (green) interacts with 5 nt of RNA (red) from the 5′ -end. After every consecutive cut EXOG looses contacts with the substrate explaining lower efficiency of cleavage for short substrates.

RNA clearance from non-flap substrates requires both EXOG and RNase H1

We further tested RNase H1 activity on a nicked, non-flap 10RNA-10DNA chimeric substrate and as expected we observed a very efficient cleavage of RNA with 1, 2 and 3 ribonucleotides left attached to the 5′ end of the DNA (Figure 2B, lanes 31–35). Conversely, EXOG showed very limited activity at the highest concentration tested (Figure 2B, lanes 26–30). It was previously shown for non-flap substrates containing 2RNA-18DNA chimeric strand that the cleavage activity of EXOG is more limited with a nick in comparison to gap-containing substrates (37). Therefore, we examined the activity of EXOG using both nick and gap substrates with downstream 10RNA-10DNA oligonucleotide (Supplementary Figure S4). The efficiency of gap substrates processing was indeed slightly enhanced in comparison to the nick substrate. However, even at the highest concentration of EXOG, a dominant product corresponded to the 18-nt band, which means that 8-nt RNA fragment remained attached to the 5′ end of the DNA. Together, the observed substrate specificity of both enzymes, RNase H1 and EXOG, is in favor of their consecutive action during the complete non-flap RNA primer removal.

EXOG-mediated RNA flap removal enables ligation of linear substrates

To test if nucleolytic activity of EXOG generates ligatable products after RNA flap removal, we purified proteins involved in RNA primer removal in human mitochondria: DNA ligase III, Pol γA, Pol γB, mtSSB and RNase H1 (Figure 3A). We then added 200nM of Lig III to reactions containing 5 nM EXOG, 150 nM Pol γ and 200 nM nick substrates with various lengths of the flap (Figure 3B and C). When the coupled cleavage-ligation reaction is successful, the 44-nt long band corresponding to the ligated product should be observed (Figure 3B). The label at the 3′ end of the flap-containing strand allowed us to distinguish the Pol γ-driven primer extension and displacement of the entire downstream oligonucleotide from the actual ligation of the product. In case of both short (2RNA) and long (15U and 15RNA) RNA flaps, we observed ligation in the presence of EXOG and Lig III (Figure 3C, lanes 4, 12 and 16, respectively), which confirms that EXOG generates optimal substrates for further nick sealing (Figure 2). The addition of Pol γ holoenzyme to these reactions resulted in slightly less efficient ligation (Figure 3C and D, lanes 5, 13 and 17, respectively). These results indicate that Pol γ may interfere with the ligation reaction but not with the cleavage of the flaps, as in each case 20-nt long bands (black arrow) which correspond to the flap-removed products of EXOG could be observed. The accumulation of the 20-mers and reduced ligation in Pol γ-containing reactions could be explained by the retention of Pol γ at the nick or Pol γ-driven partial displacement of the downstream oligonucleotide after the EXOG-mediated flap removal. Complete displacement, on the other hand, may not be the case as the displaced ssDNA would be rapidly degraded in the presence of EXOG. The substrate containing 2RNA-13DNA chimeric flap is not efficiently ligated in the presence of EXOG and Lig III (Figure 3C, lane 8). As observed in the exonuclease activity experiment (Figure 2A, lane 12–16), EXOG pauses at the RNA-DNA junction, resulting in delayed flap removal, as

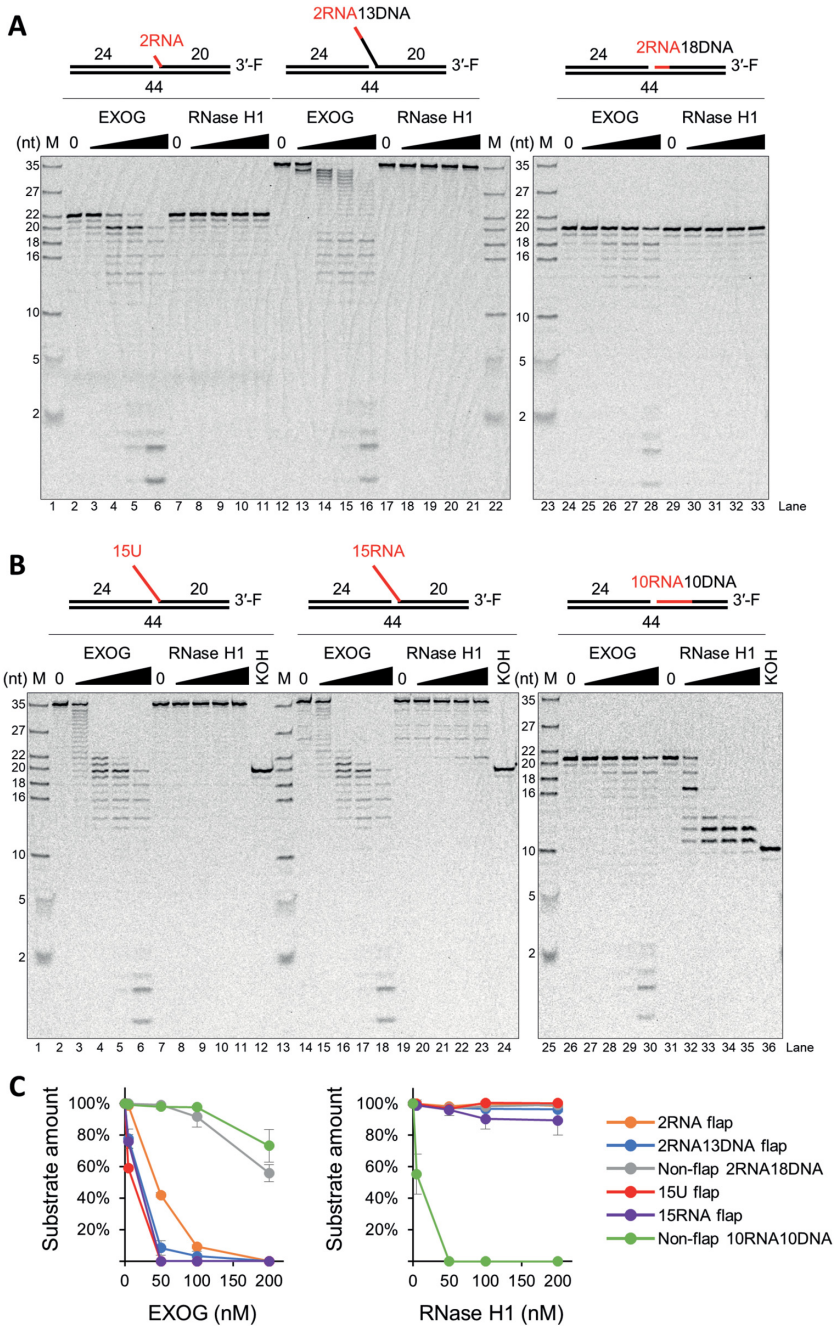

Figure 2. EXOG removes RNA from both short and long RNA-containing flaps. 200 nM of each nicked substrate (schemes of the substrates are placed at the top of the figure from left: S3, S4 and S7 in (**A**); S5, S6 and S8 in (**B**), Supplementary Table S2) was incubated with the increasing concentration of EXOG or RNase H1 (5, 50, 100, 200 nM). After 5 min of incubation, reactions were stopped and analyzed on a 23% denaturing polyacrylamide gel. Corresponding molecular weight standards are marked with M. As a control in (B), long stretches of RNA were non-enzymatically removed by KOH treatment (300 mM KOH, 55°C, 120 min). (**C**) Densitometric analysis of the decrease of tested substrates in the presence of EXOG (left) and RNase H1 (right). The graphs present the mean values with standard deviations (error bars) from two experiments.

well as excises nucleotides from the downstream DNA duplex after the flap cleavage, thus generating gaps. Both circumstances pose obstacles to Lig III activity. However, the addition of Pol γ results in increased ligation efficiency (Figure 3C and D, lane 9). Pol γ might therefore either prevent gap generation by EXOG or simply fill in the gap to form a nick for Lig III-driven sealing. We then investigated whether RNase H1 is able to support ligation of the flap substrates in the presence of Lig III and Pol γ. However, we did not observe ligation products for any substrates tested (Supplementary Figure S5). Together, EXOG in cooperation with Pol γ and Lig III promotes ligation of RNA flap-containing linear substrates, whereas RNase H1 activity does not support subsequent ligation of any substrate tested.

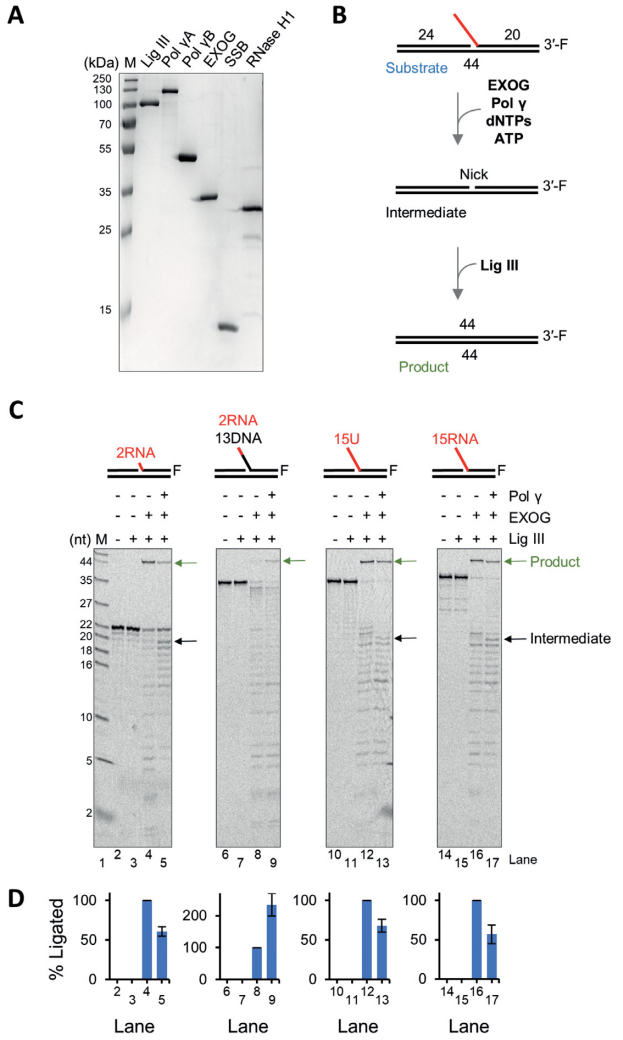

Figure 3. EXOG generates ligatable products after flap removal. (**A**) Coomassie blue-stained SDS-PAGE (15%) analysis after preparative purification of the proteins (samples of 1 μg each) used in this study. Corresponding molecular weight standards are marked with M. (**B**) Scheme of the coupled cleavage-ligation reaction on the nicked substrates with various RNA-containing flaps. (**C**) Ligation assay was performed as described in *Materials and Methods*. Schemes of the substrates are placed at the top of the figure from left: nicked substrates S3–S6, Supplementary Table S2. 200 nM of each substrate was preincubated with indicated enzymes: 200 nM Lig III, 5 nM EXOG and 150 nM Pol γ, for 10 min at 37°C in the presence of 10 mM $MgCl_2$, 1 mM ATP, 1 mM dNTPs and 1.89 μM Streptavidin, followed by the addition of unlabeled competitor DNA (C1, Supplementary Table S1). After 1h of incubation at 37°C, reactions were stopped and analyzed on a 23% denaturing polyacrylamide gel. Green arrows indicate bands corresponding to the final products of ligation, black arrows – 20-nt long intermediate products. Corresponding molecular weight standards are marked with M. (**D**) Densitometric analysis of the ligated product formation in (**C**). The value of 100% corresponds to the final product of ligation reaction including Lig III and EXOG (lanes 4, 8, 12 and 16). The graphs present the mean values with standard deviations (error bars) from two experiments.

EXOG is required for the reconstitution of primer extension coupled with ligation of circular substrates containing RNA

We also reconstituted the EXOG-assisted ligation reaction preceded by Pol γ-driven primer extension on a circular template. We used different primers with RNA-containing flaps as well as RNA or DNA non-flap 5′-ends. Circular single-stranded template (2.5 nM) was converted into a double-stranded molecule as a result of the DNA synthesis by Pol γ (12.5 nM) in the presence of mtSSB (2.5 nM). Intermediate products obtained in that fashion required 5′-end cleaning of the RNA primer and were subsequently ligated to generate the final ligated product (Figures 4A and 5A). Reactions were initiated by 20 min of Pol γ-driven DNA synthesis followed by the addition of EXOG (750 pM), RNase H1 (750 pM) and Lig III (25 nM) in various combinations (Figures 4A and 5A). The presence of [α-^{32}P] dCTP in the reactions allows to monitor primer extension by Pol γ and the separation of reactions in denaturing polyacrylamide gels enables us to distinguish the fully circular product from unligated intermediates. As a control we used 5′-phosphorylated, non-flap DNA primer and showed that Lig III alone was able to form the ligated closed circular product (Figure 4B, lane 4). The addition of RNase H1 does not affect the reaction (Figure 4B and C, lane 8). The presence of EXOG, on the other hand, removes the intermediate products (Figure 4B, compare lanes 4 and 7). RNA flap-containing circular substrates, both short and long flaps, are processed and ligated very efficiently into closed circular products exclusively in the presence of EXOG (Figure 5B, lanes 7 and 23, respectively). Similar to the linear substrates, the least efficient yet still evident ligation was observed for the substrate with 2RNA-13DNA chimeric flap (Figure 5B, lane 15). The ligation reactions remained unaffected upon the addition of RNase H1 (Figure 5B and C, lanes 8, 9, 16, 17, 24 and 25). These results indicate that EXOG is sufficient to mediate ligation of all RNA flap-containing circular substrates tested.

EXOG-RNase H1 cooperation increases the efficiency of ligation of non-flap RNA-containing substrates

In case of a non-flap RNA-containing substrate with a short 2RNA stretch at the 5′ end of the primer, EXOG mediated conversion of all intermediates into the closed circular product (Figure 4B, lane 15). No ligation was observed for RNase H1 on that substrate (Figure 4B, lanes 16). When the RNA stretch at the 5′ end of the non-flap primer was longer (15 nt), EXOG alone was also able to process it and supported closed circular product formation, albeit with lower efficiency than that on the short 2RNA non-flap substrate (Figure 4B, compare lanes 15 and 23). Again, RNase H1 alone was unable to support ligation of that substrate (Figure 4B, lane 24). However, a full conversion into the closed circular product was observed when both EXOG and RNase H1 were present in the reaction (Figure 4B and C, lane 25). To check if RNA was completely removed from the ligated products, we treated ligation reaction products of non-flap substrates with KOH, which chemically removes ribonucleotides. The comparison of KOH-treated and untreated samples (Supplementary Figure S6) demonstrates unaffected migration of bands corresponding to the ligation products, which confirms complete RNA excision.

The cooperation between EXOG and RNase H1 is required to completely remove RNA in non-flap substrates and allow for further efficient nick sealing by Lig III. To dissect the mechanism of this cooperation we examined RNA

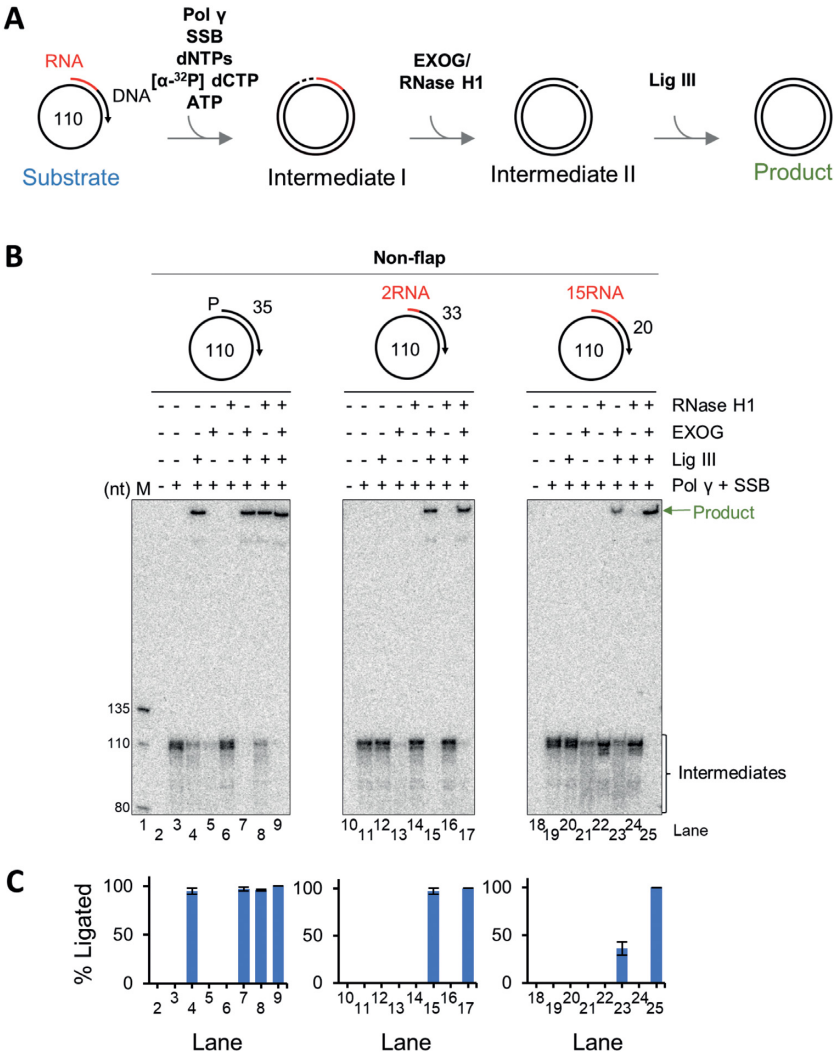

Figure 4. EXOG mediates ligation of circular RNA-containing non-flap substrates after primer extension by Pol γ. (**A**) Scheme of the primer extension-ligation reaction on the circular non-flap substrates. (**B**) Primer extension-ligation assay was performed as described in *Materials and Methods*. Schemes of the substrates are placed at the top of the figure from left: S15–S17, Supplementary Table S2. 2.5 nM of each substrate was preincubated with 12.5 nM Pol γ and 2.5 nM hmtSSB for 20 min at 37°C in the presence of 10 mM $MgCl_2$, 1 mM ATP, 0.5 μM unlabeled dNTPs and 2.5 nM [α-32P] dCTP, followed by the addition of indicated enzymes: 25 nM Lig III, 750 pM EXOG and/or 750 pM RNase H1. After 1h of incubation at 37°C, reactions were stopped and analyzed on a 12% denaturing polyacrylamide gel. Black bracket indicates bands corresponding to the intermediate products, green arrow – final products of ligation. Unlabeled substrates are not visible. Corresponding molecular weight standards are marked with M. (**C**) Densitometric analysis of the ligated closed circular product formation in (**B**). The value of 100% corresponds to the final product of ligation reaction including Pol γ, SSB, Lig III, EXOG and RNase H1 (lanes 9, 17 and 25). The graphs present the mean values with standard deviations (error bars) from two experiments.

removal pattern by titrating one enzyme against the other in the cleavage assay using a nicked, non-flap 10RNA-10DNA chimeric linear substrate (Figure 6A). As expected, RNase H1 alone leaves 1–3 RNA nucleotides (22) (Figure 6B, lanes 3–6) and EXOG has limited activity on this substrate (Figure 6C, lanes 3–6). As confirmed by base treatment (Figure 6B and C, lane 12), only when both nucleases were present, complete removal of RNA from tested substrates could be achieved (Figure 6B and C, lanes 7–11). Accumulation of RNA-free products along with the increasing concentrations of RNase H1 was exclusively observed in the presence of EXOG (Figure 6B, arrow). Similarly, the increasing concentrations of EXOG merely in the presence of RNase H1 resulted in the appearance of the same bands corresponding to the DNA products after the entire RNA removal (Figure 6C, arrow). Thus, the close coordination between EXOG and RNase H1 is necessary for total RNA clearance.

Upregulation of EXOG in mitochondria enhances ligation of RNA-containing substrates

To confirm that EXOG could be involved in the processing of nonligatable replication intermediates in mitochondria, we upregulated the levels of EXOG in human 293 cells and tested the ligation activity of corresponding mitochondrial extracts as compared to parental cells (Supplementary Figure S7). As a control, catalytically inactive EXOG-H140A (36) was overproduced. We assayed the non-flap substrate containing 2RNA-18DNA chimeric strand as well as the RNA flap-containing substrate (Fig-

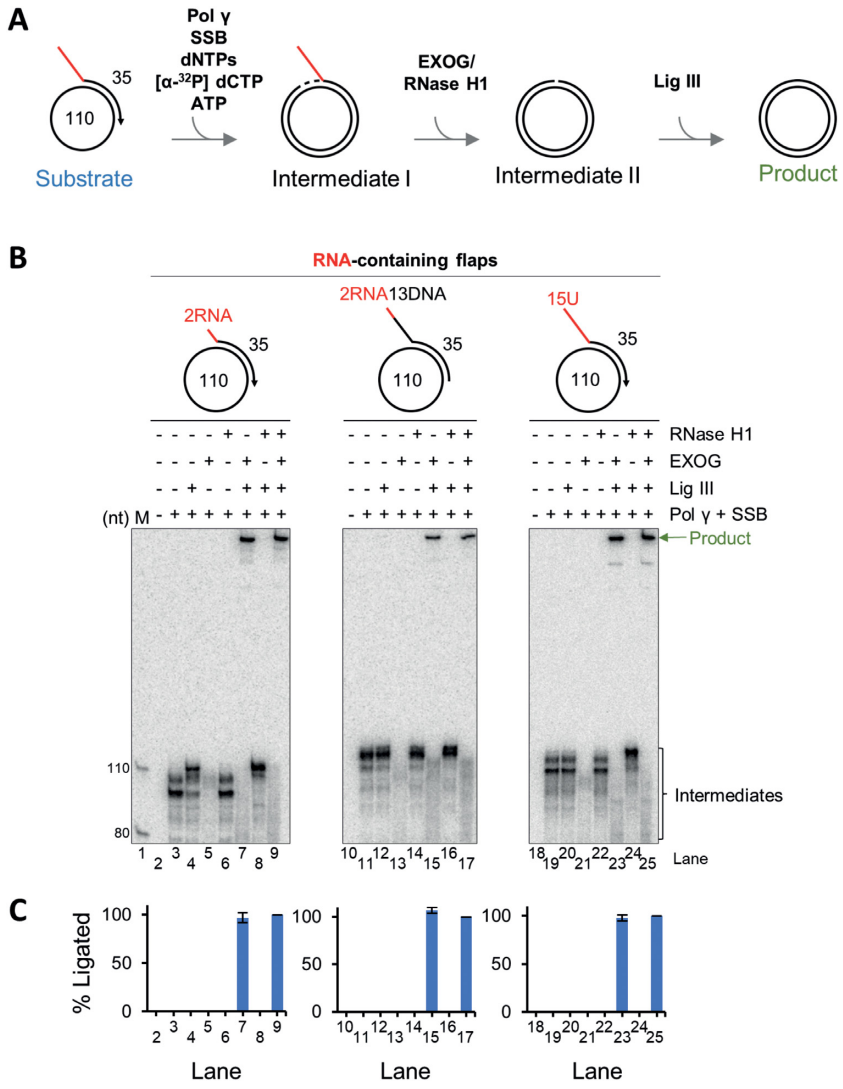

Figure 5. EXOG mediates ligation of circular substrates containing RNA flaps after primer extension by Pol γ. (**A**) Scheme of the primer extension-ligation reaction on the circular substrates with various RNA-containing flaps. (**B**) Primer extension-ligation assay was performed as described in *Materials and Methods* and in the legend to Figure 4B. Schemes of the substrates are placed at the top of the figure from left: S12–S14, Supplementary Table S2. Black bracket indicates bands corresponding to the intermediate products, green arrow – final products of ligation. Unlabeled substrates are not visible. Corresponding molecular weight standards are marked with M. (**C**) Densitometric analysis of the ligated closed circular product formation in (**B**). The value of 100% corresponds to the final product of ligation reaction including Pol γ, SSB, Lig III, EXOG and RNase H1 (lanes 9, 17 and 25). The graphs present the mean values with standard deviations (error bars) from two experiments.

ure 7A, top of the panel). We found that upregulation of active EXOG enhanced ligation of both RNA-containing substrates (Figure 7A and B). Notably, such an effect was not observed for mitochondrial extracts overproducing catalitically-inactive EXOG-H140A (Figure 7A and B), showing that the enhanced ligation of the substrates depends on EXOG-mediated nucleolytic processing. These results indicate the involvement of EXOG in RNA primer processing in mitochondria.

RNase H1 forms a complex with EXOG and other mitochondrial replication enzymes, but not with FEN1

The functional interplay between EXOG and RNase H1 prompted us to examine the possibility of a direct interaction between these two enzymes. Thus, we used microscale thermophoresis (MST) technique to test whether EXOG and RNase H1 physically interact with each other. We purified Alexa 647-labeled RNase H1 (Supplementary Figure S8A and B) and showed that labeling of RNase H1 with Alexa 647 fluorophore does not change biochemical properties of the enzyme (Supplementary Figure S8C). We then titrated Alexa 647-labeled RNase H1 with increasing concentration of unlabeled EXOG (Figure 6D). Analysis of MST binding data clearly indicate a formation of the complex between RNase H1 and EXOG with an apparent dissociation constant ($K_{d,app}$) of 22.5 ± 3.1 nM (Figure 6D and F). To ensure that the fluorescent probe does not contribute to the binding between these two enzymes, we purified Alexa 647-labeled EXOG (Supplementary Figure S9A

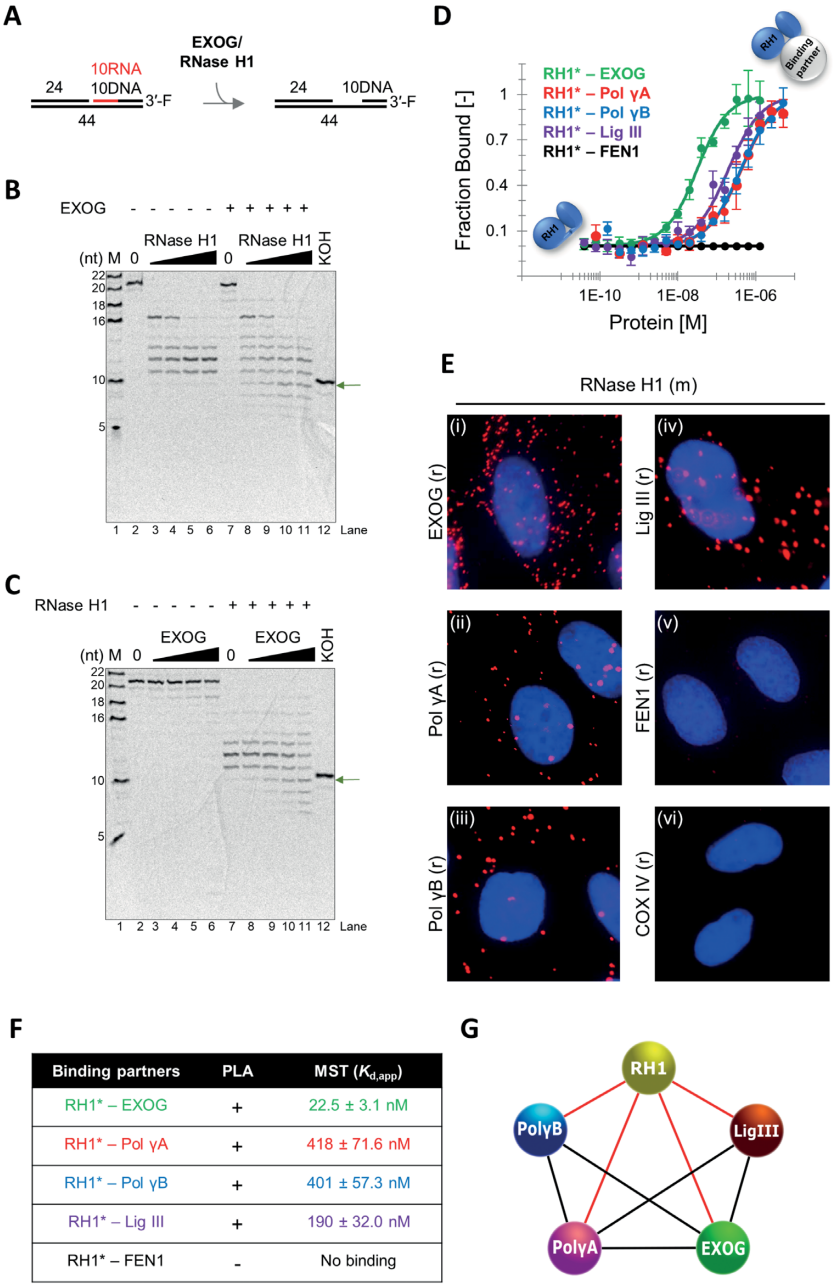

Binding partners	PLA	MST ($K_{d,app}$)
RH1* – EXOG	+	22.5 ± 3.1 nM
RH1* – Pol γA	+	418 ± 71.6 nM
RH1* – Pol γB	+	401 ± 57.3 nM
RH1* – Lig III	+	190 ± 32.0 nM
RH1* – FEN1	-	No binding

Figure 6. Coordinated action of EXOG and RNase H1 is required for complete non-flap RNA removal. Scheme of the reaction is presented in (**A**). (**B**) 200 nM of a non-flap nicked substrate (S8, Supplementary Table S2) was incubated with the increasing concentration of RNase H1 (25, 50, 100, 200 nM) in the presence or absence of EXOG (100 nM). After 5 min of incubation, reactions were stopped and analyzed on a 23% denaturing polyacrylamide gel. As a control, RNA was non-enzymatically removed by KOH treatment (300 mM KOH, 55°C, 120 min). An arrow indicates bands corresponding to the RNA-free products. Corresponding molecular weight standards are marked with M. (**C**) Reactions performed as described in (**B**) with the increasing concentration of EXOG (25, 50, 100, 200 nM) in the presence or absence of RNase H1 (100 nM). (**D**) Thermophoresis signal of the titration of RNase H1 (~10 pM–320 nM) against 2 nM Alexa 647-labeled EXOG. Fit of the changes in thermophoresis signal to a single-site binding model yield K_d of 9.9 ± 2.2 nM. Error bars indicate the standard deviation of a triplicate of experiments. (**E**) The interaction of RNase H1 with EXOG, Pol γA, Pol γB, Lig III or FEN1 was investigated using PLA in human lung epithelial cells. The primary antibodies of two different species are indicated (m – mouse; r – rabbit). The specificity of the interaction was monitored by the interaction between RNase H1 and the mitochondrial protein marker COX IV (mitochondrial inner membrane protein). Representative images of at least two independent experiments are shown. (**F**) Table summarizing results from MST. (**G**) Protein interaction network for enzymes involved in human mitochondrial RNA primer removal. Red line – novel interactions identified in this work; black lines – previously known protein–protein interactions.

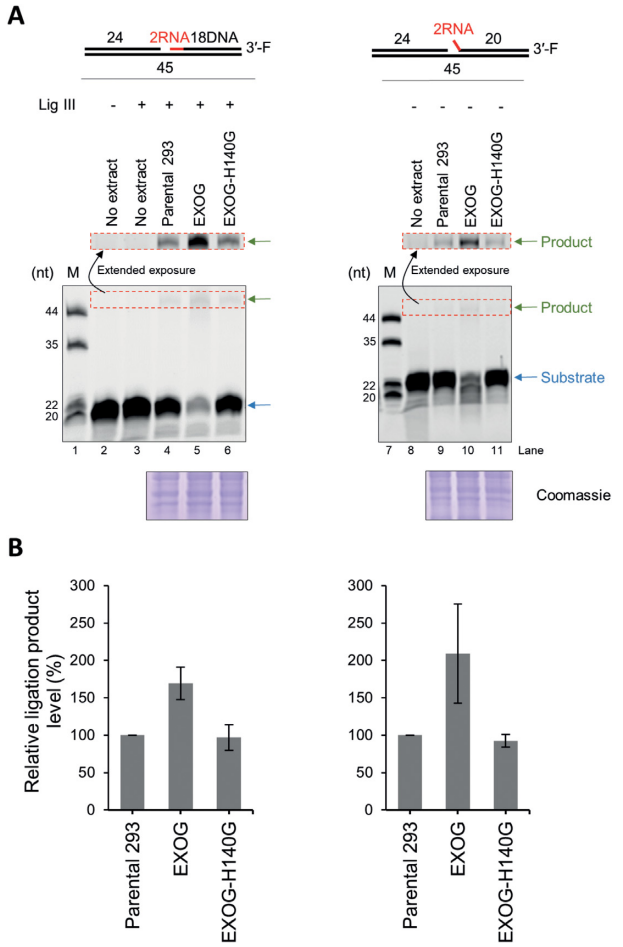

Figure 7. EXOG overproduction improves ligation of RNA-containing substrates in mitoplast extracts. (**A**) Results of ligation assay with RNA-containing substrates and mitoplast extracts. The assay was performed as described in *Materials and Methods*. Schemes of the substrates are placed at the top of the figure (from left: S18 and S19 Supplementary Table S2). The reactions with non-flap substrate (left) were supplemented with Lig III. The upper box represents the same boxed area as the gel below but with extended exposure. Coomassie blue-stained SDS-PAGE analysis of mitoplast extracts was applied to confirm that equal amounts of the samples were used for the reactions. Green arrows indicate bands corresponding with final products of ligation, blue arrows – substrates. Corresponding molecular weight standards are marked with M. (**B**) Densitometric analysis of the ligation product formation in (A). The value of 100% corresponds to the product of ligation reaction for control parental 293 cells (lanes 4 and 9). The graph presents the mean values with standard deviations (error bars) from at least two biological repeats.

and B) and performed reverse titration where Alexa 647-labeled EXOG was titrated with increasing concentration of unlabeled RNase H1. Similar value of an apparent dissociation constant ($K_{d,app} = 9.9 \pm 2.2$ nM) provides the evidence that the interaction between EXOG and RNase H1 is specific (Supplementary Figure S9C). The labeling of EXOG also does not affect its enzymatic activity (Supplementary Figure S9D).

To test whether a mere presence of either enzyme or its catalytic activity is necessary for the successful RNA primer removal we purified catalytically inactive variants of EXOG (EXOG-H140G, Supplementary Figures S1 and S10; (36)) and RNase H1 (RNase H1-D210N, Supplementary Figure S3; (49)) and tested the RNA removal in the cleavage assay using nucleolytically inactive variants so that one enzyme of the pair was inactive. As hypothesized, the presence of nucleolytically inactive variants of each enzyme resulted in incomplete RNA removal (Supplementary Figure S11A-C). This effect was not due to the loss of protein-protein interactions between inactive variant of one enzyme and the wild-type variant of the other as an apparent dissociation constant did not appear to be significantly altered ($K_{d,app}$ of 5.8 ± 2.0 nM and 3.0 ± 1.0 nM for EXOG-H140G-wt RNase H1 and wt EXOG-RNase H1-D210N, respectively; Supplementary Figure S11D).

EXOG was previously shown to interact with Pol γ and Lig III (33,50). Using MST, we investigated possible complex formation between RNase H1 and these enzymes. We titrated Alexa 647-labeled RNase H1 with increasing concentration of unlabeled Pol γA, Pol γB and Lig III (Figure 6D). Indeed, we observed the binding of both Pol γA ($K_{d,app} = 418 \pm 71.6$ nM) and Pol γB ($K_{d,app} = 401 \pm 57.3$ nM) as well as Lig III ($K_{d,app} = 190 \pm 32.0$ nM) to RNase H1 (Figure 6D and F). Since FEN1 was previously proposed to be involved in mitochondrial primer removal (23), we also analyzed the possible complex formation of FEN1 with RNase H1 and EXOG. We purified FEN1 (Supplementary Figure S12A and B) and confirmed its specific endonuclease activity towards flap-containing substrates (Supplementary Figure S12C). Both Alexa-labeled RNase H1 and EXOG were titrated with increasing concentrations of unlabeled FEN1. Even at the highest concentrations of FEN1 no binding to either RNase H1 (Figure 6D and F) or EXOG was detected (Supplementary Figure S13A).

To provide direct evidence for the biological significance of newly discovered interactions, we used the Proximity Ligation Assay (PLA) approach which allows the detection of close proximity/interaction between two proteins *in cellulo* based on antibody specificity. We detected interactions between RNase H1 and EXOG, Pol γA, Pol γB, and Lig3 (Figure 6E, i–iv and S14) in human lung epithelial BEAS 2B cells. However, we did not observe interactions either between RNase H1 and FEN1 (Figure 6E, v and S14) or EXOG and FEN1 (Supplementary Figure S13B, i and S14). The specificity of the assay was confirmed by lack of interaction between RNase H1 and the subunit of the cytochrome c oxidase (COX IV) located in the inner mitochondrial membrane (Figure 6E, vi and S14), while strong signal was observed for interaction between EXOG and dsDNA (mtDNA) (Supplementary Figures S13B, ii and S14). Our PLA results are in agreement with *in vitro* MST results, showing that RNase H1 forms a complex not only with EXOG but also with both subunits of Pol γ as well as Lig III, whereas FEN1 interacts with neither EXOG nor RNase H1. Together, the reconstituted primer extension-ligation reactions (Figure 4) along with the cleavage assay and MST/PLA binary interaction studies strongly indicate functional and physical interactions between EXOG and RNase H1, and support the proposed mechanism of cooperation between both enzymes in the flap-independent pathway of RNA primer removal in mitochondria.

FEN1 is not observed in mitochondrial fractions of the human lung epithelial cells

Reports on mitochondrial localization of FEN1 are contradictory and argue about its role in mtDNA processing (29,30,51–53). Since our *in vitro* and *in cellulo* results demonstrate that FEN1 is not interacting with either RNase H1 or EXOG, we investigated a submitochondrial localization of FEN1 in non-tumorigenic derived cells. Crude mitochondria isolated from the human lung epithelial cells (BEAS 2B) were further separated into two fractions containing the outer membrane with intermembrane space proteins and inner membrane with matrix proteins using protocol described in (47). The fractions purity was tested using mitochondrial translocase of the outer membrane subunit 22 (TOM22) and translocase of the inner membrane subunit 22 (TIM22) that are localized in the outer and inner mitochondrial membrane, respectively (Supplementary Figure S13C). In addition, we tested localization of cytochrome c and α subunit of ATP synthase that localized in the intermembrane space/inner membrane and inner membrane, respectively (Supplementary Figure S13C). mtDNA together with proteins involved in replication and repair of the mtDNA are localized in the mitochondrial matrix in close proximity to the inner mitochondrial membrane (54). We detected RNase H1, EXOG, catalytic and accessory subunits of Pol γ and Lig III but not FEN1 to localize mostly in the inner membrane/mitochondrial matrix fraction (Supplementary Figure S13C). FEN1 was hardly detectable in both mitochondrial fractions, while it was readily detected in whole cell extract and cytosolic fraction. The faint signal of FEN1 in the inner membrane/mitochondrial matrix fraction may represent contamination, alike faint signal for cytoplasmic marker, β-actin. Our combined results indicate that FEN1 involvement in replication of the mtDNA in human lung epithelial cells seems unlikely.

DISCUSSION

A search for the nuclease involved in primer removal during mtDNA replication and a broad spectrum of substrates recognized and processed by EXOG (36,37) led us to hypothesize that this enzyme, exclusively located in mitochondria, could be a perfect candidate for RNA primer removal activity. It was previously suggested that a FEN1-like activity is needed for primer removal in mitochondria (23) favoring a flap-dependent pathway of primer removal during DNA replication in mitochondria. However, the Pol γ-mediated RNA displacement was shown to be limited in *in vitro* assay (10) and the flap formation by Pol γ *in vivo* is still debated. On the other hand, recently published *in vitro* cleavage results showed that EXOG can specifically excise RNA dinucleotide at the junction of RNA and DNA in a duplex (37), thus having a potential to provide an alternative flap-independent pathway of primer removal after the initial RNase H1-catalysed cleavage. Whether EXOG activity leads to the formation of ligatable ends has not been elucidated.

In this work, we demonstrate that EXOG cleaves very efficiently and accurately single-stranded RNA flaps of various lengths (2 and 15 nt) and, in concert with Pol γ and Lig III, generates ligated products. Additionally, we observed that the ligation efficiency of the substrate containing RNA flap is enhanced in mitochondrial extracts where enzymatically active EXOG is overproduced (Figure 7, right panel). If short RNA flap could be further displaced by Pol γ, a chimeric RNA-DNA flap would be generated. EXOG processes chimeric flaps as well albeit with lower efficiency as it pauses at the RNA-DNA junction. Nevertheless, in our reconstituted primer extension-ligation reaction with the circular template containing chimeric flap, we observed the formation of ligated product in the presence of EXOG (Figure 5). Possibly, the activity of another mitochondrial nuclease, e.g. MGME1, DNA flap-specific enzyme (10), could further increase the efficiency of the chimeric flap removal and thus the ligation reaction. Alternatively, the pausing of EXOG at the RNA-DNA junction during the cleavage of chimeric flaps, together with exonuclease activity of Pol γ, could allow reannealing of the displaced DNA to the template strand. As a result, it is plausible that mere RNA clearance from a chimeric flap could be sufficient to generate ligatable substrate for Lig III. This scenario remains to be verified, as the chimeric flap of the substrate in our experiments was not complementary to the template.

FEN1 and Dna2 are nucleases involved in the flap cleavage during Okazaki fragments maturation of the lagging strand in eukaryotic nuclear DNA replication (24–28). Two main pathways of this process were proposed (for recent reviews, refer to (55–57)): primary, short-flap pathway involving FEN1, and the secondary, less frequent pathway that removes 'runaway' longer flaps via the combined activity of Dna2, FEN1 and a single-stranded DNA-binding protein RPA (26). Here we show that EXOG participates in both short and long RNA flap removal which may occur during the mtDNA processing, and thus combines the activities of FEN1 and Dna2 into one enzyme. Moreover, we found that not only does FEN1 interact with neither RNase H1 nor EXOG, but also it is absent from mitochondria of human lung epithelial cells. Our results explain previously reported lack of effect of FEN1 depletion on OriL ligation *in vivo* (23). Since Dna2 contains a non-canonical MTS and was shown to localize to mitochondria (53,58), it could either cooperate with EXOG or otherwise affect processing of the longer flaps during mitochondrial primer removal.

We demonstrated that alternative model for non-flap RNA removal also works efficiently. It requires a consecutive action of both EXOG and RNase H1 to excise RNA primer and obtain the ligated product thus providing evidence of the non-redundant function of both enzymes. Importantly, KOH-treatment of the products reveals no residual ribonucleotides, confirming that cooperation of EXOG with RNase H1 leads to complete removal of the RNA primer. Moreover, we observed that upregulation of enzymatically active EXOG in mitochondrial extracts increases the ligation efficiency of the substrate containing a short fragment of RNA that is not further processed by RNase H1 (Figure 7, left panel). Finally, our MST binding studies and results of our PLA *in cellulo* proximity/interactions confirmed the physical interaction between EXOG and RNase H1. As enzymatic activity of both enzymes is critical for complete RNA removal, it suggests that EXOG and RNase H1 could act together as a complex on the

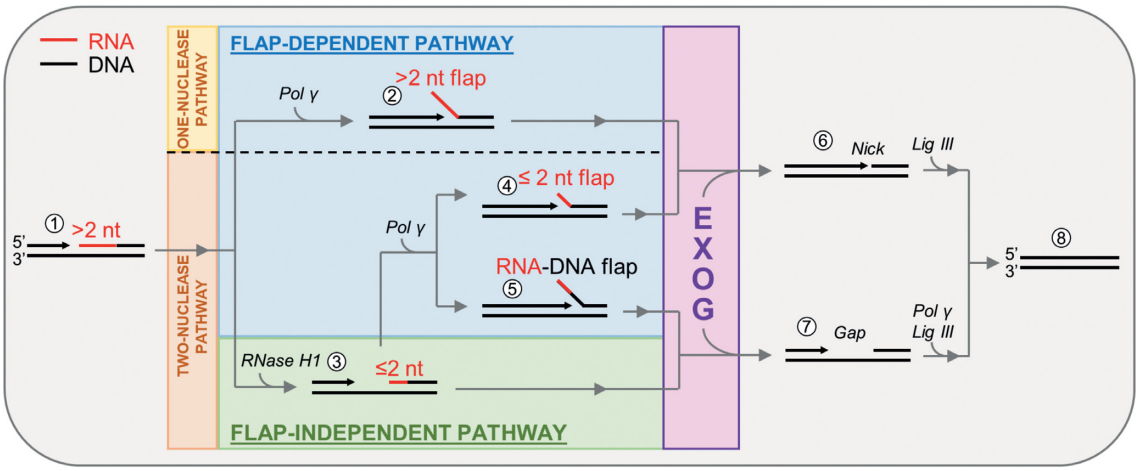

Figure 8. Model for possible pathways of mitochondrial RNA primer removal. RNA primer longer than 2 nucleotides (1) can be either displaced by Pol γ, creating a long RNA flap (2), or partially cleaved by RNase H1, leaving a few ribonucloetides at the 5′ end of DNA (3). Both intermediate products are immediately processed by EXOG to remove remaining RNA. Alternatively, Pol γ displaces a short RNA fragment after RNase H1 processing, thus generating either a short RNA flap (4) or RNA–DNA chimeric flap (5). Both flaps are cleaved by EXOG. In case of flaps consisting solely of RNA (2 and 4), EXOG-mediated flaps removal generates optimal product (6) for final ligation (8). The non-flap RNA primer (3) processing as well as the RNA–DNA chimeric flap (5) excision produce gaps (7) that require the gap-filling activity of Pol γ before ligation reaction. The model assumes that the flap-dependent pathway is served by either one or two nucleases. The flap-independent pathway requires the activity of both nucleases.

common substrate. Reconstituted by us *in vitro* complete RNA primer removal pathway is a multi-step process and requires coordinated action of proteins with different enzymatic properties. A complex formation between Pol γA, Pol γB, Lig III and EXOG have been previously shown (33,50,59). Here we report the novel interaction between RNase H1 and EXOG as well as Pol γA, Pol γB and Lig III (Figure 6G). Synchronized action of all these proteins within a large multienzyme machine may be necessary to catalyze multiple transactions required to process the RNA primer and terminate mtDNA replication. Identification of the minimal set of mitochondrial enzymes necessary for the complete RNA primer removal *in vitro* offers the possibility to examine the effect of detrimental and compensatory patient-derived mutations identified in those enzymes on the efficiency of entire RNA primer removal pathway.

In conclusion, we show that EXOG is a multifunctional mitochondrial ribonuclease which facilitates the removal of RNA primer and supports the ligation of RNA-free ends. Our findings let us to propose a model of possible pathways that lead to the RNA primer removal and ligation during mtDNA replication (Figure 8). This includes the flap-dependent pathway, which requires a strand-displacement activity of Pol γ, as well as the flap-independent pathway, where a coordinated action of EXOG and RNase H1 is required. The cleavage of long RNA flaps could be merely dependent on the activity of EXOG. Since Pol γ possesses limited strand-displacement activity (9–11), multiple repetition of Pol γ-driven displacement and EXOG-mediated removal of short/medium-length RNA flaps are feasible to contribute to the primer removal in mitochondria. When RNA primer is partially processed by RNase H1 and a few ribonucleotides are still attached to the 5′-end of DNA, the remaining RNA fragment may or may not be displaced by Pol γ into a short RNA or RNA–DNA chimeric flap. Regardless the pathway, the nucleolytic activity of EXOG removes RNA remnants allowing for subsequent ligation by Lig III.

DATA AVAILABILITY

ImageJ is an open-source image processing and analysis software (http://rsb.info.nih.gov/ij/).

SUPPLEMENTARY DATA

Supplementary Data are available at NAR Online.

ACKNOWLEDGEMENTS

We thank Marcin Nowotny (IIMCB) for plasmid of RNase H1, Patrick J. O'Brien (University of Michigan) for plasmid of Lig III and Jane A. Grasby (University of Sheffield) for plasmid of FEN1. We thank Danuta Gutowska-Owsiak (University of Gdansk), Lukasz Borowski (University of Warsaw) and members of the Szymanski lab for discussions and critical reading of the manuscript.

FUNDING

POIR.04.04.00–00-3E44/17 project, carried out within the First TEAM programme of the Foundation for Polish Science co-financed by the European Union under the European Regional Development Fund; National Science Centre, Poland [UMO-2016/21/P/NZ1/01085]; European Union's Horizon 2020 research and innovation programme under the Marie Skłodowska-Curie [665778], as a part of POLONEZ Fellowship; M.R.S. was supported by the Ministry of Education and Science, Poland and the EMBO Installation Grant [4129]; work of R.J.S. and J.C. was supported by POIR.04.04.00–00-5E63/18-00 project, carried out within the First TEAM programme of the Foundation

for Polish Science co-financed by the European Union under the European Regional Development Fund. Funding for open access charge: University of Gdansk.
Conflict of interest statement. None declared.

REFERENCES

1. Zeviani,M. and Di Donato,S. (2004) Mitochondrial disorders. *Brain*, **127**, 2153–2172.
2. Young,M.J. and Copeland,W.C. (2016) Human mitochondrial DNA replication machinery and disease. *Curr. Opin. Genet. Dev.*, **38**, 52–62.
3. Larsson,N.-G., Wang,J., Wilhelmsson,H., Oldfors,A., Rustin,P., Lewandoski,M., Barsh,G.S. and Clayton,D.A. (1998) Mitochondrial transcription factor A is necessary for mtDNA maintance and embryogenesis in mice. *Nat. Genet.*, **18**, 231–236.
4. Copeland,W.C. and Longley,M.J. (2014) Mitochondrial genome maintenance in health and disease. *DNA Repair (Amst.)*, **19**, 190–198.
5. Spelbrink,J.N., Toivonen,J.M., Hakkaart,G.A., Kurkela,J.M., Cooper,H.M., Lehtinen,S.K., Lecrenier,N., Back,J.W., Speijer,D. and Foury,F. (2000) In vivo functional analysis of the human mitochondrial DNA polymerase POLG expressed in cultured human cells. *J. Biol. Chem.*, **275**, 24818–24828.
6. Longley,M.J., Prasad,R., Srivastava,D.K., Wilson,S.H. and Copeland,W.C. (1998) Identification of 5′-deoxyribose phosphate lyase activity in human DNA polymerase γ and its role in mitochondrial base excision repair in vitro. *Proc. Natl. Acad. Sci.*, **95**, 12244–12248.
7. Johnson,A.A., Tsai,Y.-c., Graves,S.W. and Johnson,K.A. (2000) Human mitochondrial DNA polymerase holoenzyme: reconstitution and characterization. *Biochemistry*, **39**, 1702–1708.
8. Graziewicz,M.A., Longley,M.J. and Copeland,W.C. (2006) DNA polymerase γ in mitochondrial DNA replication and repair. *Chem. Rev.*, **106**, 383–405.
9. He,Q., Shumate,C.K., White,M.A., Molineux,I.J. and Yin,Y.W. (2013) Exonuclease of human DNA polymerase gamma disengages its strand displacement function. *Mitochondrion*, **13**, 592–601.
10. Uhler,J.P., Thörn,C., Nicholls,T.J., Matic,S., Milenkovic,D., Gustafsson,C.M. and Falkenberg,M. (2016) MGME1 processes flaps into ligatable nicks in concert with DNA polymerase γ during mtDNA replication. *Nucleic Acids Res.*, **44**, 5861–5871.
11. Farge,G., Pham,X.H., Holmlund,T., Khorostov,I. and Falkenberg,M. (2007) The accessory subunit B of DNA polymerase γ is required for mitochondrial replisome function. *Nucleic Acids Res.*, **35**, 902–911.
12. Macao,B., Uhler,J.P., Siibak,T., Zhu,X., Shi,Y., Sheng,W., Olsson,M., Stewart,J.B., Gustafsson,C.M. and Falkenberg,M. (2015) The exonuclease activity of DNA polymerase γ is required for ligation during mitochondrial DNA replication. *Nat. Commun.*, **6**, 7303.
13. Falkenberg,M. (2018) Mitochondrial DNA replication in mammalian cells: overview of the pathway. *Essays Biochem.*, **62**, 287–296.
14. Yasukawa,T. and Kang,D. (2018) An overview of mammalian mitochondrial DNA replication mechanisms. *J. Biochem.*, **164**, 183–193.
15. Robberson,D.L., Kasamatsu,H. and Vinograd,J. (1972) Replication of mitochondrial DNA. Circular replicative intermediates in mouse L cells. *Proc. Nat. Acad. Sci. U.S.A.*, **69**, 737.
16. Kasamatsu,H. and Vinograd,J. (1973) Unidirectionality of replication in mouse mitochondrial DNA. *Nat. New Biol.*, **241**, 103–105.
17. Wolstenholme,D.R., Koike,K. and Cochran-Fouts,P. (1973) Single strand-containing replicating molecules of circular mitochondrial DNA. *J. Cell Biol.*, **56**, 230–245.
18. Cotner-Gohara,E., Kim,I.-K., Hammel,M., Tainer,J.A., Tomkinson,A.E. and Ellenberger,T. (2010) Human DNA ligase III recognizes DNA ends by dynamic switching between two DNA-bound states. *Biochemistry*, **49**, 6165–6176.
19. Holt,I.J. (2009) Mitochondrial DNA replication and repair: all a flap. *Trends Biochem. Sci*, **34**, 358–365.
20. Uhler,J.P. and Falkenberg,M. (2015) Primer removal during mammalian mitochondrial DNA replication. *DNA Repair (Amst.)*, **34**, 28–38.
21. Holmes,J.B., Akman,G., Wood,S.R., Sakhuja,K., Cerritelli,S.M., Moss,C., Bowmaker,M.R., Jacobs,H.T., Crouch,R.J. and Holt,I.J. (2015) Primer retention owing to the absence of RNase H1 is catastrophic for mitochondrial DNA replication. *Proc. Natl. Acad. Sci. U.S.A.*, **112**, 9334–9339.
22. Lima,W.F., Rose,J.B., Nichols,J.G., Wu,H., Migawa,M.T., Wyrzykiewicz,T.K., Siwkowski,A.M. and Crooke,S.T. (2007) Human RNase H1 discriminates between subtle variations in the structure of the heteroduplex substrate. *Mol. Pharmacol.*, **71**, 83–91.
23. Al-Behadili,A., Uhler,J.P., Berglund,A.-K., Peter,B., Doimo,M., Reyes,A., Wanrooij,S., Zeviani,M. and Falkenberg,M. (2018) A two-nuclease pathway involving RNase H1 is required for primer removal at human mitochondrial OriL. *Nucleic Acids Res.*, **46**, 9471–9483.
24. Budd,M.E. and Campbell,J.L. (1997) A yeast replicative helicase, Dna2 helicase, interacts with yeast FEN-1 nuclease in carrying out its essential function. *Mol. Cell. Biol.*, **17**, 2136–2142.
25. Bae,S.-H. and Seo,Y.-S. (2000) Characterization of the enzymatic properties of the yeast dna2 Helicase/endonuclease suggests a new model for Okazaki fragment processing. *J. Biol. Chem.*, **275**, 38022–38031.
26. Bae,S.-H., Bae,K.-H., Kim,J. and Seo,Y.-S. (2001) RPA governs endonuclease switching during processing of Okazaki fragments in eukaryotes. *Nature*, **412**, 456–461.
27. Ayyagari,R., Gomes,X.V., Gordenin,D.A. and Burgers,P.M. (2003) Okazaki fragment maturation in yeast. I. Distribution of functions between FEN1 and DNA2. *J. Biol. Chem.*, **278**, 1618–1625.
28. Kao,H.-I., Veeraraghavan,J., Polaczek,P., Campbell,J.L. and Bambara,R.A. (2004) On the roles of *Saccharomyces cerevisiae* Dna2p and Flap endonuclease 1 in Okazaki fragment processing. *J. Biol. Chem.*, **279**, 15014–15024.
29. Akbari,M., Visnes,T., Krokan,H.E. and Otterlei,M. (2008) Mitochondrial base excision repair of uracil and AP sites takes place by single-nucleotide insertion and long-patch DNA synthesis. *DNA Repair (Amst.)*, **7**, 605–616.
30. Szczesny,B., Tann,A.W., Longley,M.J., Copeland,W.C. and Mitra,S. (2008) Long patch base excision repair in mammalian mitochondrial genomes. *J. Biol. Chem.*, **283**, 26349–26356.
31. Szczesny,R.J., Hejnowicz,M.S., Steczkiewicz,K., Muszewska,A., Borowski,L.S., Ginalski,K. and Dziembowski,A. (2013) Identification of a novel human mitochondrial endo-/exonuclease Ddk1/c20orf72 necessary for maintenance of proper 7S DNA levels. *Nucleic Acids Res.*, **41**, 3144–3161.
32. Cymerman,I.A., Chung,I., Beckmann,B.M., Bujnicki,J.M. and Meiss,G. (2008) EXOG, a novel paralog of endonuclease G in higher eukaryotes. *Nucleic Acids Res.*, **36**, 1369–1379.
33. Tann,A.W., Boldogh,I., Meiss,G., Qian,W., Van Houten,B., Mitra,S. and Szczesny,B. (2011) Apoptosis induced by persistent single-strand breaks in mitochondrial genome: critical role of EXOG (5′-EXO/endonuclease) in their repair. *J. Biol. Chem.*, **286**, 31975–31983.
34. Szczesny,B., Olah,G., Walker,D.K., Volpi,E., Rasmussen,B.B., Szabo,C. and Mitra,S. (2013) Deficiency in repair of the mitochondrial genome sensitizes proliferating myoblasts to oxidative damage. *PLoS One*, **8**, e75201.
35. Xiao,J., Dong,X., Peng,K., Ye,F., Cheng,J., Dan,G., Zou,Z., Cao,J. and Sai,Y. (2021) PGC-1α Mediated-EXOG, a specific repair enzyme for mitochondrial DNA, plays an essential role in the rotenone-induced neurotoxicity of PC12 cells. *J. Mol. Neurosci.*, **71**, 2336–2352.
36. Szymanski,M.R., Yu,W., Gmyrek,A.M., White,M.A., Molineux,I.J., Lee,J.C. and Yin,Y.W. (2017) A domain in human EXOG converts apoptotic endonuclease to DNA-repair exonuclease. *Nat. Commun.*, **8**, 14959.
37. Wu,C.-C., Lin,J.L.J., Yang-Yen,H.-F. and Yuan,H.S. (2019) A unique exonuclease ExoG cleaves between RNA and DNA in mitochondrial DNA replication. *Nucleic Acids Res.*, **47**, 5405–5419.
38. Longley,M.J., Smith,L.A. and Copeland,W.C. (2009) Preparation of human mitochondrial single-stranded DNA-binding protein. *Methods Mol. Biol.*, **554**, 73–85.
39. Nowotny,M., Gaidamakov,S.A., Ghirlando,R., Cerritelli,S.M., Crouch,R.J. and Yang,W. (2007) Structure of human RNase H1 complexed with an RNA/DNA hybrid: insight into HIV reverse transcription. *Mol. Cell*, **28**, 264–276.
40. McNally,J.R. and O'Brien,P.J. (2017) Kinetic analyses of single-stranded break repair by human DNA ligase III isoforms

reveal biochemical differences from DNA ligase I. *J. Biol. Chem.*, **292**, 15870–15879.
41. Szymanski,M.R., Kuznetsov,V.B., Shumate,C., Meng,Q., Lee,Y.S., Patel,G., Patel,S. and Yin,Y.W. (2015) Structural basis for processivity and antiviral drug toxicity in human mitochondrial DNA replicase. *EMBO J.*, **34**, 1959–1970.
42. Dosekova,P., Dubiel,A., Karlowicz,A., Zietkiewicz,S., Rydzanicz,M., Habalova,V., Pienkowski,V.M., Skirkova,M., Han,V., Mosejova,A. *et al.* (2020) Whole exome sequencing identifies a homozygous POLG2 missense variant in an adult patient presenting with optic atrophy, movement disorders, premature ovarian failure and mitochondrial DNA depletion. *Eur. J. Med. Genet.*, **63**, 103821.
43. Zillner,K., Jerabek-Willemsen,M., Duhr,S., Braun,D., Längst,G. and Baaske,P. (2012) In: *Functional Genomics*. Springer, pp. 241–252.
44. Jerabek-Willemsen,M., André,T., Wanner,R., Roth,H.M., Duhr,S., Baaske,P. and Breitsprecher,D. (2014) MicroScale thermophoresis: interaction analysis and beyond. *J. Mol. Struct.*, **1077**, 101–113.
45. Szczesny,R.J., Kowalska,K., Klosowska-Kosicka,K., Chlebowski,A., Owczarek,E.P., Warkocki,Z., Kulinski,T.M., Adamska,D., Affek,K. and Jedroszkowiak,A. (2018) Versatile approach for functional analysis of human proteins and efficient stable cell line generation using FLP-mediated recombination system. *PLoS One*, **13**, e0194887.
46. Kotrys,A.V., Cysewski,D., Czarnomska,S.D., Pietras,Z., Borowski,L.S., Dziembowski,A. and Szczesny,R.J. (2019) Quantitative proteomics revealed C6orf203/MTRES1 as a factor preventing stress-induced transcription deficiency in human mitochondria. *Nucleic Acids Res.*, **47**, 7502–7517.
47. Nishimura,N. and Yano,M. (2014) Separation of the inner and outer mitochondrial membrane in HeLa cells. *Bio.-protocol.*, **4**, e1299.
48. Richards,E.G., Flessel,C.P. and Fresco,J.R. (1963) Polynucleotides. VI. Molecular properties and conformation of polyribouridylic acid. *Biopolymers*, **1**, 431–446.
49. Wu,H., Lima,W.F. and Crooke,S.T. (2001) Investigating the structure of human RNase H1 by site-directed mutagenesis. *J. Biol. Chem.*, **276**, 23547–23553.
50. Szczesny,B., Brunyanszki,A., Olah,G., Mitra,S. and Szabo,C. (2014) Opposing roles of mitochondrial and nuclear PARP1 in the regulation of mitochondrial and nuclear DNA integrity: implications for the regulation of mitochondrial function. *Nucleic Acids Res.*, **42**, 13161–13173.
51. Liu,P., Qian,L., Sung,J.-S., de Souza-Pinto,N.C., Zheng,L., Bogenhagen,D.F., Bohr,V.A., Wilson,D.M. III, Shen,B. and Demple,B. (2008) Removal of oxidative DNA damage via FEN1-dependent long-patch base excision repair in human cell mitochondria. *Mol. Cell. Biol.*, **28**, 4975–4987.
52. Kazak,L., Reyes,A., He,J., Wood,S.R., Brea-Calvo,G., Holen,T.T. and Holt,I.J. (2013) A cryptic targeting signal creates a mitochondrial FEN1 isoform with tailed R-Loop binding properties. *PLoS One*, **8**, e62340.
53. Zheng,L., Zhou,M., Guo,Z., Lu,H., Qian,L., Dai,H., Qiu,J., Yakubovskaya,E., Bogenhagen,D.F. and Demple,B. (2008) Human DNA2 is a mitochondrial nuclease/helicase for efficient processing of DNA replication and repair intermediates. *Mol. Cell*, **32**, 325–336.
54. Holt,I.J., He,J., Mao,C.-C., Boyd-Kirkup,J.D., Martinsson,P., Sembongi,H., Reyes,A. and Spelbrink,J.N. (2007) Mammalian mitochondrial nucleoids: organizing an independently minded genome. *Mitochondrion*, **7**, 311–321.
55. Burgers,P.M. and Kunkel,T.A. (2017) Eukaryotic DNA replication fork. *Annu. Rev. Biochem.*, **86**, 417–438.
56. Stodola,J.L. and Burgers,P.M. (2017) Mechanism of lagging-strand DNA replication in eukaryotes. *DNA Replication*, **1042**, 117–133.
57. Balakrishnan,L. and Bambara,R.A. (2013) Okazaki fragment metabolism. *Cold Spring Harb. Perspect. Biol.*, **5**, a010173.
58. Duxin,J.P., Dao,B., Martinsson,P., Rajala,N., Guittat,L., Campbell,J.L., Spelbrink,J.N. and Stewart,S.A. (2009) Human Dna2 is a nuclear and mitochondrial DNA maintenance protein. *Mol. Cell. Biol.*, **29**, 4274–4282.
59. Lim,S.E., Longley,M.J. and Copeland,W.C. (1999) The mitochondrial p55 accessory subunit of human DNA polymerase γ enhances DNA binding, promotes processive DNA synthesis, and confers N-ethylmaleimide resistance. *J. Biol. Chem.*, **274**, 38197–38203.